Zhao *et al. Carbon Research* (2025) 4:64
https://doi.org/10.1007/s44246-025-00228-2

Carbon Research

ORIGINAL ARTICLE

Open Access

Soil–plant-microbial evidence for the available phosphorus generation and utilization of Ca/Mg salts conditioned hydrochar from sewage sludge

Qian Zhao[1], Wei Guo[1*], Yuhan Zhu[1], Dongyue Li[1], Xiaohui Liu[2*], Minda Yu[3], Dongyang Li[4], Xiang Gao[5], Xishi Tai[5] and Jun Li[1]

Abstract

Metal salts-modified sewage sludge (SS) biochar is increasingly used in agricultural soil remediation, although its effects on available phosphorus (P) species, plant growth and microbial communities remain unclear. This study prepared CaO, $CaCl_2$, MgO and $MgCl_2$-modified hydrochars derived from SS at 260 °C for 2 h. Then the available P characteristics of the hydrochars and their effects on the growth of *Vigna radiata* (mung bean) and soil microorganisms were comprehensively evaluated by chemical extraction, pot experiments and the diffusive gradients in thin-films (DGT) technique. Results indicated that Ca-based hydrochars contained more slow-release apatite P (AP) compounds (e.g., $Ca_5(PO_4)_3OH$, $Ca_5(PO_4)_3Cl$ and Ca_2PO_4Cl), with a 48.6%–86.3% increase in AP content compared to the control at 260 °C. In contrast, Mg-based hydrochars were richer in easy-release AP compounds (e.g., $Mg_3(PO_4)_2$ and $Ca_3Mg_3(PO_4)_4$), with a lower AP increase of 0–50.7%. Compared with Ca salts modified hydrochars, Mg-modified hydrochars (especially MgO) were more effective for the promotion of rapid growth, chlorophyll synthesis and photosynthesis in *V. radiata* plants, resulting in more P accumulation within mung beans, which was consistent with the P release results obtained by DGT. The addition of Ca-modified hydrochars promoted the enrichment of bacterial communities such as *Skermanella* and *RB41*, which was helpful for improving the mineralization and circulation of P in soil. While the addition of Mg-modified hydrochars to soils enhanced the activity of P-solubilizing bacteria such as *Pseudomonas* and *Bacillus*, which was conducive to the dissolution and utilization of P. This highlights Ca-based hydrochars as a stable long-term P source and Mg-based hydrochars for rapid plant uptake, offering a novel strategy for P fertilizer application.

*Correspondence:
Wei Guo
gwfybj@bjut.edu.cn
Xiaohui Liu
lxh7786@ouc.edu.cn
Full list of author information is available at the end of the article

Springer

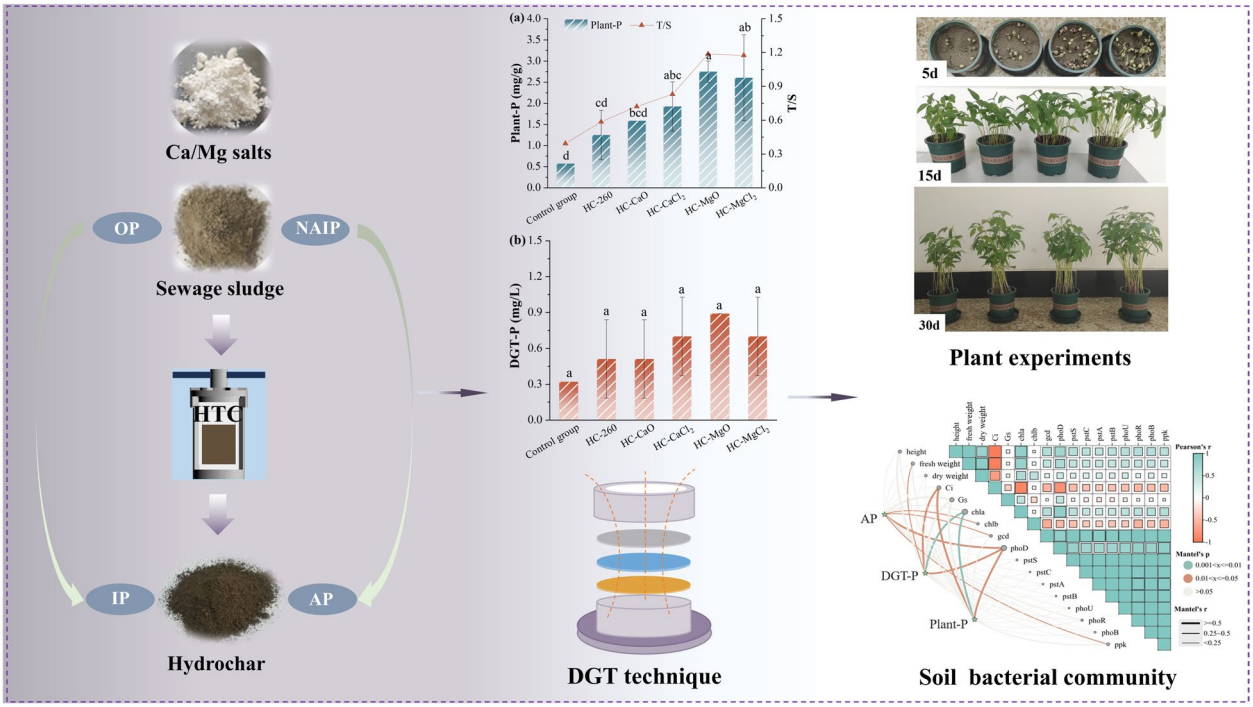
© The Author(s) 2025. **Open Access** This article is licensed under a Creative Commons Attribution 4.0 International License, which permits use, sharing, adaptation, distribution and reproduction in any medium or format, as long as you give appropriate credit to the original author(s) and the source, provide a link to the Creative Commons licence, and indicate if changes were made. The images or other third party material in this article are included in the article's Creative Commons licence, unless indicated otherwise in a credit line to the material. If material is not included in the article's Creative Commons licence and your intended use is not permitted by statutory regulation or exceeds the permitted use, you will need to obtain permission directly from the copyright holder. To view a copy of this licence, visit http://creativecommons.org/licenses/by/4.0/.

Highlights

- Ca/Mg salts promoted the transformation of P from Al-P and Fe–P to Mg-P and Ca-P.
- Mg-based hydrochars offer rapid uptake P and boost P-solubilizing bacterial activity.
- Ca-based hydrochars provide long-term available P and enhance soil bacterial communities for P mineralization.
- Mg-modified hydrochars are more effective for promoting mung bean growth.

Keywords Sewage sludge, Hydrothermal carbonization, Calcium/magnesium salts, Phosphorus species, Plant growth, Microbial community

Graphical Abstract



1 Introduction

Phosphorus (P) is an indispensable element in living organisms, for the progression of genetic processes, molecule synthesis and energy storage (Elser 2012). Currently, more than 90% of P resources are derived from finite phosphate rock reserves (Mnthambala et al. 2021), which are rapidly depleting and unevenly distributed. Depletion is predicted to occur within 100 years at current consumption rates (Yogev et al. 2020), and the extreme concentration of 70%–75% of known reserves (~ 50 billion tons) in Morocco creates strategic dependence on importing countries (El Bamiki et al. 2021). It is estimated that by 2050, more than 5.7 billion people will be facing P scarcity (White et al. 2010). Sewage sludge (SS), a by-product of wastewater treatment process, containing various essential nutrients and organic Matter, with P contents typically ranging from 15.8 to 28.8 mg/g (Chen et al. 2022a), Making SS a promising alternative P resource. Municipal sludge is produced in significant quantities, with countries Like the United States, China, and India generating 12.7, 7.8 and 4.0 million tons of dry sewage sludge (SS) annually, respectively (Liu et al. 2021a). Given the substantial global production of SS, the phosphate present in SS recovered from wastewater treatment plants (WWTPs) has the potential to meet 40% to 50% of the phosphate requirements (Egle et al. 2016). Consequently, P recovery from SS has received major interest as an important, sustainable and renewable source of P.

Hydrothermal carbonization (HTC) of SS has attracted significant attention as a low-environmental impact, low-energy consuming and well-established method for sludge management (Ma et al. 2025; Li et al. 2025). Previous research has confirmed that HTC can obtain a stable proportion of phosphate-containing minerals (hydroxyapatite) (> 90%), which cannot be achieved by incineration or pyrolysis under the same conditions (Fang et al. 2023). Studies have demonstrated that P was mainly concentrated in hydrochar, presenting as inorganic P (IP) after HTC treatment (Zheng et al. 2020b). More than 80% of the P initially present in raw SS is retained within hydrochar, primarily as orthophosphate, which is the desirable form for phosphate fertilizer utilization (Wang et al. 2019; Fang et al. 2023). When applied as a soil amendment, hydrochar exhibits an excellent capacity for nutrient retention and pH buffering (Wang et al. 2019). Additionally, HTC does not require a drying step in practical sludge disposal and re-utilization processes, significantly reducing operational costs.

The structure and composition of phosphate in hydrochar are known to affect its bioavailability as a phosphate resource (Ghosh et al. 2015), i.e., the proportion of P readily available for plant uptake. The metal cations in SS (such as Ca^{2+}, Mg^{2+}, Al^{3+} and Fe^{3+}), form different apatite substances with P during the HTC process (Pan et al. 2007). For example, when oxides and hydroxides of Al and Fe are present in SS, the P in hydrochar exists mainly in the form of non-apatite inorganic P (NAIP) (Xu et al. 2018). However, the tight binding of high concentrations of Al^{3+} and Fe^{3+} to phosphate may lead to biological damage following the use of hydrochar as a phosphate fertilizer (Li et al. 2019). When SS contains high concentrations of Mg^{2+} and Ca^{2+} compounds, phosphate in hydrochar mainly exists as apatite phosphorus (AP) (Adam et al. 2009), which is more beneficial for organisms within the ecosystem to absorb and utilize P and has lower toxicity than NAIP (Wu et al. 2020). Therefore, the method of regulating the formation of hydrochar from SS through the addition of Ca and Mg ions has broad application prospects for the utilization of hydrochar as a phosphate fertilizer. Current studies have shown that the addition of Ca/Mg salts such as CaO, MgO, $CaCl_2$ and $MgCl_2$, can promote the conversion of NAIP to AP in SS incineration products, improving the bioavailability of P in solid-phase products (Li et al. 2019; Xu et al. 2021). Notable differences have been reported in the transformation and effectiveness of different Ca and Mg salts. For example, Ca salts such as CaO and $CaCl_2$, tend to form stable phosphate compounds, such as $Ca_5(PO_4)_3OH$ and Ca_2PO_4Cl, significantly enhancing P availability, while MgO and $MgCl_2$ are more likely to form highly bioavailable Mg-phosphate compounds, such as $Mg_3(PO_4)_2$ and $Ca_3Mg_3(PO_4)_4$. However, the impact of Ca/Ma salts on P speciation and bioavailability in SS following HTC treatment is still unclear. Previous research on the preparation of SS-based hydrochar, has mainly focused on the material hydrothermal characteristics and biochar properties (Nahar et al. 2024; Liu et al. 2025a, b), while major knowledge gaps remain in terms of the use of hydrothermal carbonization for efficient P reuse.

Studies evaluating the P availability of hydrochar have mostly focused on the analysis of some representative available P compounds and the evaluation of P availability within hydrochar by stimulating the secretion of organic acids by plants (Zhu et al. 2022). However, direct evidence regarding the utilization of P in hydrochar by plants remains scarce. Typically, the traditional methods used for the process of assessing P utilization in hydrochar, include destructive sampling techniques and chemical analysis (Jordan-Meille et al. 2012), which change the soil environment, thereby affecting the accuracy in estimating the available P uptake capacity of plants during soil hydrochar applications. When hydrochar is applied to the soil as P fertilizer, in addition to the P uptake characteristics of plants, plant growth characteristics and changes in the soil microbial community also require attention. It is important that these problems are explored to comprehensively evaluate the scientific and engineering application value of hydrochar as a P fertilizer after the treatment of SS by HTC. Diffusive gradients in thin-films (DGT) is a passive sampling technique that mimics the ion absorption process by plant roots, better reflecting P uptake by plant than traditional chemical extraction methods (Vogel et al. 2017). Therefore, combining soil pot experiments with DGT analysis can effectively overcome the shortcomings of these individual methods for the analysis of SS hydrochar as a phosphate fertilizer, allowing the mechanism of regulation of different Ca/Mg salts on the P conversion and utilization of SS hydrochar, to be further explored.

Therefore, based on the results of hydrothermal tests, pot experiments and DGT analysis, this study investigated the fate of Ca/Mg salts (including CaO, $CaCl_2$, MgO and $MgCl_2$) modified hydrochar derived from SS, when used as a phosphate fertilizer for soil amelioration. The aims of the current work are to 1) clarify the role of Ca/Mg salts in the conversion of P through the standards, measurements and testing (SMT) analysis and the characterization of P species in the Ca/Mg conditioned hydrochar; 2) assess the impact of hydrochar on P bioavailability in soils by combining chemical

extraction and DGT analysis; 3) determine the impact of hydrochar on plant biomass and physiological characteristics under controlled conditions; and 4) analyze the changes of soil microbial composition following hydrochar application through the high-throughput sequencing of 16S rRNA genes.

2 Materials and methods

2.1 Materials and chemicals

The raw SS used in this experiment was dewatered sludge from a WWTP in Binzhou City (Shandong Province, China [37°25′N, 118°01′E]). Sludge was dewatered using a vacuum freeze dryer (FD-1A-50, Bo Yi Kang Instrument Co., Beijing, China). The constant-weight sludge was then ground and sieved through a 100-mesh screen to obtain uniform particles, which were then stored in a dryer for hydrothermal treatment. The basic elemental composition of the SS sample is outlined in Table S1 (Supplementary Materials). To analyze the modified hydrochar-induced change of soil properties and plant growth, a pot experiment was performed with *Vigna radiata* (mung bean) plants, using hydrochar as a fertilizer. The soil used for experiments was collected from the top soil layer (10–20 cm depth) in the southeast Chaoyang District of Beijing (China [116°25′E, 39°58′N]), the chemical properties of which are outlined in the Supplementary Materials, Table S2. The soil is a typical agricultural soil, the average annual rainfall is 581 mm, and the annual average temperature is 11.6°C. The chemical reagents used in this study are detailed in Supplementary Materials, Text S1.

2.2 Hydrochar preparation and P fraction analysis

2.2.1 Hydrochar preparation

Dry SS and deionized water were added to a high-pressure hydrothermal reactor at a ratio of 1:9 (w:v) and heated to 260 °C for 2 h. The HTC temperature (260 ℃) was selected based on the results of preliminary experiments (Supplementary Materials, Fig. S1), as it not only maximized AP enrichment but also promoted the formation of structurally stable and potentially plant-available P species. The hydrochar sample derived from SS without Ca/Mg salts was labeled 'HC-260'. For other hydrochar samples, Ca/Mg salts (CaO, $CaCl_2$, MgO and $MgCl_2$) were mechanically dry mixed at Mass ratios of 2.5, 5, or 10% for co-hydrothermal treatment with sludge, based on the results of previous research (Xu et al. 2018). The prepared hydrochar samples labeled according to their salt-loading ratio, e.g., CaO-2.5% represent hydrochar produced through HTC of SS with 2.5% ratios of CaO at 260 °C.

2.2.2 Analysis of P speciation in hydrochar

The P within the SS/hydrochar was detected following the SMT program (González Medeiros et al. 2005). According to this method, P in SS/hydrochar was categorized into five forms: total P (TP), organic P (OP), IP, AP (bound to Ca/Mg) and NAIP (bound to Al/Mn/Fe), with TP calculated as the sum of OP and IP, while IP was calculated as the sum of NAIP and AP. The P content was quantified by the molybdenum blue method with UV–vis spectrophotometry measurements (Murphy and Riley 1962). Detailed SMT procedures are provided in the Supplementary Materials (Fig. S2).

2.2.3 Characterization of hydrochar

The surface morphology of the sludge and hydrochars was observed by scanning electron microscopy (SEM, ZEISS GeminiSEM 300). The specific surface area and pore structure use the Brunauer–Emmett–Teller (BET) method (Micromeritics Tristar II 3020). X-ray diffraction (XRD) was conducted to identify the crystalline phase of P compounds in the raw SS and derived hydrochar samples (Zhang et al. 2024). X-ray photoelectron spectroscopy (XPS) was employed to investigate the chemical states and bonding environments of P in hydrochar samples. The detailed methodology used for XRD and XPS analysis is described in Text S2. Fourier transform infrared spectroscopy (FTIR, Thermo Fisher Scientific Nicolet iS20) was applied to characterize the chemical functional groups of sludge and hydrochars.

2.3 Heavy metal fractionation analysis

To evaluate the ecological safety of Ca/Mg-modified hydrochar, the chemical speciation of six representative heavy metals (Cd, Pb, Cr, Cu, Zn, and Ni) was analyzed using a sequential extraction method based on the modified BCR (European Community Bureau of Reference) protocol (Meng et al. 2018). This method fractionates metals into four operationally defined categories: exchangeable (F1), reducible (F2), oxidizable (F3), and residual (F4) fractions. The environmental immobility of heavy metals follows the order of F4 > F3 > F2 > F1. Fractions F1 and F2 are considered directly toxic due to high mobility, F3 is potentially toxic owing to the degradability of organic matter, and F4 is regarded as non-toxic and stable (Zhao et al. 2024). Metal concentrations in each fraction were determined using inductively coupled plasma optical emission spectrometry (ICP-AES; Optima8300, USA). The fractionation results were used to evaluate the environmental mobility and bioavailability of metals in the hydrochar.

2.4 Plant growth characteristics and the available P content of hydrochar

2.4.1 Pot experiments

The amount of available P corresponds to the fertilization efficiency of P within the soil, directly affecting the growth of legumes and crop yields. Therefore, various studies have selected legumes as model plants to study the relationship between plant characteristics and soil P efficiency (Ghimirey et al. 2024). To investigate the performance of the prepared hydrochar as a phosphate fertilizer on plant growth characteristics, pot experiments were carried out using *V. radiata* as the representative legume plant. Before experiments, mung bean seeds were screened to eliminate substandard seeds. The seeds were then subjected to surface disinfection by 1% (v/v) sodium hypochlorite solution, and then washed with sterile distilled water to remove residual disinfectant. Based on the analysis of available P after soil samples were mixed with hydrochar, a 2% addition was determined to be the optimal ratio for hydrochar addition to soil as a phosphate fertilizer (Text S3, Fig. S3). Then, six groups of pot experiments were conducted, including one control group without the addition of hydrochar and five experimental groups with hydrochar added, such as HC-260, CaO-5%, $CaCl_2$−5%, MgO-5% and $MgCl_2$−5%. Each experimental group consisted of 3 parallel treatments to ensure the reliability of experimental results. The pots had a upper diameter of 11.1 cm and a height of 9.9 cm. Each pot was filled approximately 500 g of soil or soil-2% hydrochar (w/w). Before use, the soil was dried and sieved following the method described in Sect. 2.3.1. The *V. radiata* seeds were pre-germinated for 7-day period, with 20 seeds sown in each pot for culturing, followed by uniform harvesting and plant characterization after 30 d. Photographic images of *V. radiata* plants fertilized using hydrochar in the pot experiments are shown in Supplementary Materials, Fig. S4.

2.4.2 Plant growth characteristics

To evaluate the impacts of different modified hydrochars on plant physiological properties, the photosynthetic gas exchange parameters of *V. radiata* plants were determined before being harvested, using a portable infrared gas exchange analyzer (LI–6400 XT, Licor, USA). The intercellular carbon dioxide concentration (C_i) refers to the carbon dioxide levels between cells and stomatal conductance (G_s) refers to the degree of stomatal openness in plant leaves, both of which affect photosynthesis and crop water use, ultimately affecting overall crop yields and productivity (Cheng et al. 2024).

After harvesting, fresh *V. radiata* plants were removed from the soil. The height of the plant was measured from the base of the stem to the tallest apical bud using a caliper. The average height was calculated from three randomly selected plants per treatment group. The selected plants were then thoroughly washed with distilled water and immediately weighed. The fresh biomass was then cut into small pieces, dehydrated to a constant dry weight at 75 °C for 36 h and the dry weights were recorded. Chlorophyll content was measured using the dimethyl sulfoxide (DMSO) method (Hiscox and Israelstam 1979). Briefly, 0.1 g of fresh leaf biomass was mixed with 5 mL of DMSO, and then heated at 65 °C until the leaf discs became completely colorless. The absorbance of the chlorophyll extracts was measured at 649 and 665 nm, using DMSO as the sample blank.

2.4.3 Optimization of the proportion of hydrochar added to soil

The Olsen method is widely used to assess plant-available P in soils, as this extraction method has been shown to correlate strongly with plant P uptake (Zehetner et al. 2018). In this work, the available P content was determined approximately one week after the obtained hydrochar (HC-260, HC-CaO, HC-$CaCl_2$, HC-MgO and HC-$MgCl_2$) was combined with soil at varying loading ratios of 1%, 2% and 3%. According to the results of P speciation analysis in hydrochar obtained through the addition of Ca/Mg salts, a 5% addition ratio was found to obtain the highest content of AP, and therefore, hydrochar with a 5% Ca/Mg salts addition ratio was selected for all subsequent experiments. Before the pot experiment, the test soil was collected from the plough layer (10–20 cm) of an agricultural field, air-dried at room temperature, ground, and sieved through a 2 mm mesh. Hydrochar samples produced (HC260, CaO-5%, $CaCl_2$−5%, MgO-5% and $MgCl_2$−5%) were mixed with the soil at Mass-based loading ratios of 1%, 2%, and 3% (w/w, dry weight basis). Each treatment was set up in triplicate. The impacts of hydrochar loading ratios of 1%, 2% and 3% on soil P availability were then compared to determine the optimal soil loading ratio (Text S3, Fig. S3). The available P content of soils (Olsen-P) was measured following the Danish standard method for P analysis (Text S4). P concentrations were monitored using the method of P determination described in Sect. 2.2.2.

2.4.4 P analysis in soils and plants

Total P content in soil (Soil-P) was measured before pot experiments by digesting the samples with a mixture of concentrated sulfuric acid (H_2SO_4) and perchloric acid ($HClO_4$), following the method outlined by Lu (2000). For *V. radiata* P content (Plant-P), the NY/T 2421–2013 standard method was applied. The Soil-P and Plant-P concentrations were determined using the molybdenum blue method (Murphy and Riley 1962). All experiments

were conducted in triplicate. The methods are described in detail in the Supplementary Materials (Text S4).

2.4.5 Determination of available P in soils

DGT was employed to assess soil P bioavailability by measuring the kinetically labile P pool through dynamic diffusion and adsorption processes (Six et al. 2012). The DGT device consists of a binding layer and a diffusive gel layer. Upon deployment, labile P species (e.g., $H_2PO_4^-$, HPO_4^{2-}) diffuse through the diffusive layer and are irreversibly captured by the binding gel, establishing a localized depletion zone that mimics plant root uptake. The accumulated P mass is converted to an effective concentration using the DGT equation, which accounts for diffusive boundary layer thickness and deployment time. This approach provides a time-integrated measurement of P resupply capacity from soil solids to solution, reflecting both solution P and the buffer capacity of solid-phase P (Santner et al. 2012; Mason et al. 2013). The detail of the methods is given in Supplementary Text S4.

2.5 Microbial analysis of the soil rhizosphere zone with the addition of hydrochar

The plant rhizosphere zone is considered to be the main region of interaction between plants and soils (Guan et al. 2015), as a key area for microbial activity and nutrient (such as N and P) utilization by plants. Therefore, in this study, the soil within the rhizospheric zone of *V. radiata* was collected to reveal the impact of various hydrochars on microbial community within this region. In order to analyze the composition and diversity of soil microbial communities, 16S rRNA sequencing was carried out using the Illumina NovaSeq PE250 platform (Shenzhen, China) (Wu et al. 2025). Finally, the function of the obtained data was predicted based on Picrust2 software. The detailed procedures followed are given in the Supplementary Materials (Text S5).

2.6 Statistical analysis

Statistical analysis was performed using SPSS 26.0 for Windows, with the results presented as mean values ± standard deviation. The data was analyzed using a one-way analysis of variance (ANOVA) followed by Tukey's test ($p < 0.05$). All of the sludge sample analyses were conducted in triplicate.

3 Results and discussion

3.1 Effect of adding Ca/Mg salts on the composition and speciation of P in hydrochars

3.1.1 Composition of P in hydrochars

Figure 1 shows the different P fractions (IP, OP, AP, and NAIP) in hydrochars with and without the addition of Ca/Mg salts. As depicted in Fig. 1a, the content of OP in HC-260 was comparatively low, accounting for only 4.9% of the TP content (Table S3, Supplementary Materials), which is consistent with previous findings that the HTC process favors the retention of IP rather than OP (Shi et al. 2019; Zheng et al. 2020a). With increased dosages of CaO/MgO, the IP content decreased gradually and the decrease in IP concentration in hydrochars was associated with an increase in hydrochar yield (Table S4, Supplementary Materials). As shown in Fig. 1a, the hydrochar samples prepared with $CaCl_2$/$MgCl_2$ had higher IP concentrations than those prepared with CaO/MgO. As shown in Table S4 (Supplementary Materials), a significant mass loss occurred when a Cl-donor was added to SS during HTC treatment (Jeon and Kim 2018). Furthermore, most P-containing compounds in the hydrochar were non-volatile, leading to an increase in P content per unit mass of hydrochar.

Upon addition of metal salts, the distribution of AP and NAIP in hydrochars was changed, and the different cations (Ca^{2+} vs. Mg^{2+}) and anions (O^{2-} vs. Cl^-) resulted in a variation in the content of AP and NAIP in hydrochars (Fig. 1b). Specifically, the concentrations of AP and NAIP in the hydrochar sample prepared without salts were 14.6 ± 0.5 mg/g and 12.6 ± 0.3 mg/g. When adding 5% CaO or $CaCl_2$, the concentrations of AP increased from 14.6 mg/g to 27.2 or 26.5 mg/g ($p < 0.05$), while the NAIP content decreased from 12.6 mg/g to 0 or 5.8 mg/g ($p < 0.05$), respectively, which is in accordance with the results of previous studies (Zheng et al. 2020a, b; Han et al. 2021). Results showed that Ca-modified HTC treatment could significantly and effectively promote the conversion of NAIP to AP. However, when the added amount of CaO or $CaCl_2$ was increased further, the AP content of hydrochars decreased, consistent with findings reported by Li et al. (2019) previously, showing that the AP content did not increase when the Ca:P ratio exceeded 1. Compared with the complete transformative effect of CaO on AP, chloride ions in $CaCl_2$ may affect the precipitation and dissolution equilibrium of phosphates through competitive coordination or by changing the ionic strength of the solution, leading to variation in the distribution of P forms (House 1999). However, further increasing the amount of CaO or $CaCl_2$ added led to a decrease in AP concentration in the hydrochar, indicating that excessive levels of addition did not enhance the transformation of NAIP to AP.

The addition of MgO or $MgCl_2$ During HTC also facilitated the conversion of NAIP to AP. As the amount of MgO increased, the AP concentration rose from 14.6 mg/g (without MgO) to 22.0 mg/g (with 10% MgO) ($p < 0.05$). However, with increased levels of MgO addition, the NAIP content decreased continuously. The AP content of hydrochar fluctuated slightly with increased

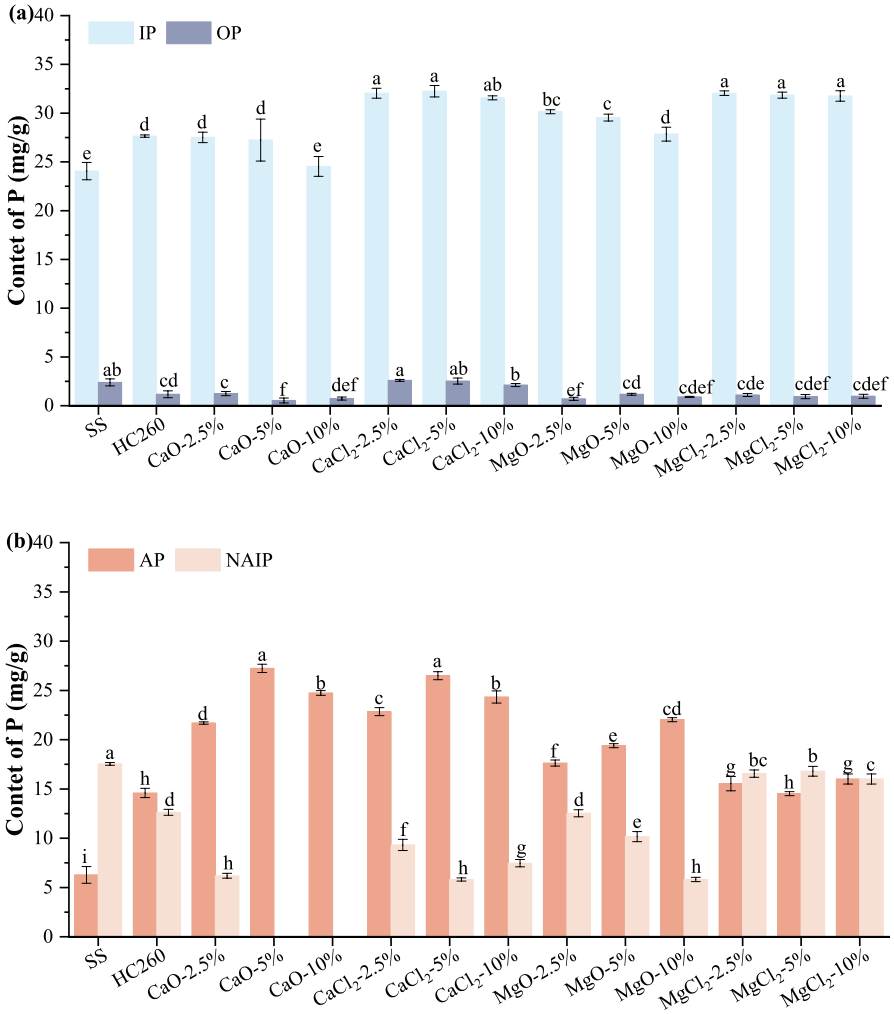


Fig. 1 P composition in hydrochars produced with different Ca and Mg salts using the SMT method: **a** IP and OP concentrations; **b** AP and NAIP concentrations. Letters indicate significant differences among the treatments using Tukey post hoc test

$MgCl_2$ addition dosages. Previous work reported by Fang et al. (2021) similarly noted that the AP concentration of $MgCl_2$-treated sludge biochars was less than 20 mg/g. The addition of Mg salts may have facilitated the reaction between phosphate and Mg ions, producing relatively soluble Mg phosphate minerals, which may explain the increase in AP concentration. However, the weaker binding capacity of Mg^{2+} to P compared to Ca^{2+} may have resulted in relatively low AP concentrations and high NAIP levels in Mg-treated hydrochar (Li et al. 2019). Overall, the influence of Mg salts on the conversion of NAIP to AP was not as significant ($p < 0.05$) as that of Ca salts, due to the lower stability of the formed phosphate minerals. Existing research emphasized the enhancement of the transformation from NAIP to AP to increase P bioavailability in sludge-derived biochar. However, the AP content is not equivalent to bioavailable P levels. Many studies relied on the excessive additions of calcium-based or biomass-derived amendments, but the bioavailability of various Ca-Mg-P minerals produced has not been discussed.

3.1.2 Morphology and P speciation of hydrochars

The SEM images (Fig. 2) and BET analysis results (Table 1, Fig. S5) collectively reveal significant morphological and textural variations among the samples, reflecting the impact of hydrothermal treatment and salt modification on sludge-derived hydrochar. The raw SS sample presents a dense and irregular surface, while hydrothermal treatment at 260 °C (HC260) results in a more compact and slightly porous structure, accompanied by increased BET surface area and pore volume (Table 1). This improvement was attributed to the release of gases (e.g., CO_2, H_2S) from the decomposition of unstable components, which creates pores and surface cracks (Du et al. 2021). The addition of CaO/$CaCl_2$

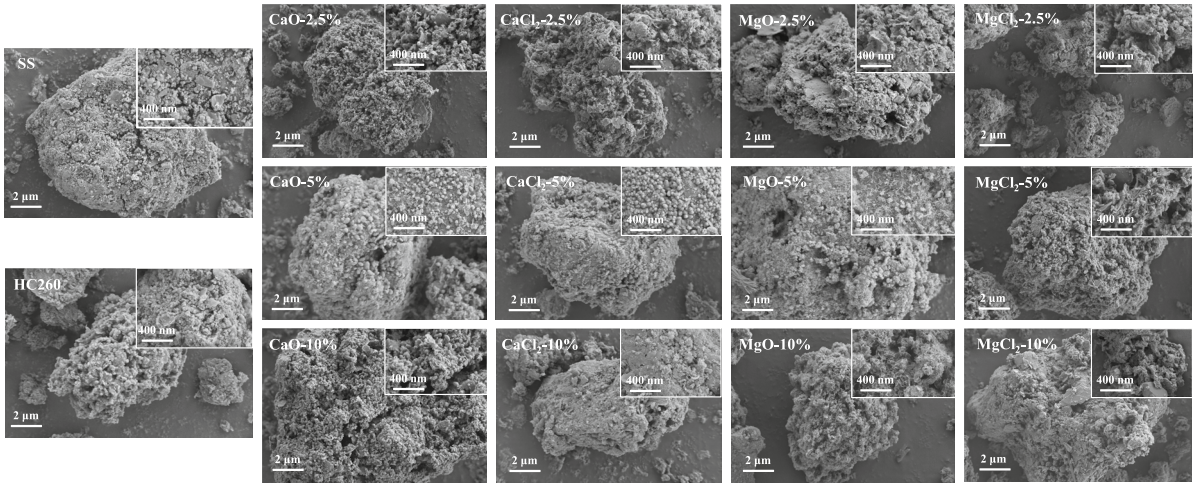


Fig. 2 SEM diagram of raw SS and hydrochar prepared using different salt dosages

Table 1 Surface area and pore distribution properties of the samples

Samples	BET surface area (m^2/g)	Pore volume (cm^3/g)	Pore diameter (nm)
SS	22.34	0.099	17.08
HC260	35.07	0.17	18.91
CaO–2.5%	32.63	0.16	19.11
CaO–5%	41.24	0.17	15.95
CaO–10%	38.12	0.16	16.29
$CaCl_2$–2.5%	33.22	0.12	14.52
$CaCl_2$–5%	35.81	0.16	17.49
$CaCl_2$–10%	34.75	0.17	19.29
MgO–2.5%	43.25	0.20	18.38
MgO–5%	71.44	0.29	15.82
MgO–10%	99.01	0.44	17.9
$MgCl_2$–2.5%	31.21	0.14	18.39
$MgCl_2$–5%	30.73	0.15	20.10
$MgCl_2$–10%	32.47	0.15	19.04

promotes the formation of aggregated crystalline structures on the surface, indicating effective P mineralization. Correspondingly, BET results show moderate increases in surface area, with CaO-5% achieving the highest value among calcium-modified samples (41.24 m^2/g), while pore diameters remain relatively unchanged. In contrast, MgO-treated samples exhibit flake-like structures under SEM, conducive to phosphate adsorption (Wang et al. 2025), and exhibit the most significant improvements in surface area and pore volume, especially MgO-10%, exhibiting the most significant improvement, with a surface area of 99.01 m^2/g and a pore volume of 0.44 cm^3/g. The addition of $MgCl_2$ results in a fragmented and highly porous texture, aligning with their larger pore diameters observed in BET analysis.

The crystalline characteristics of the prepared hydrochars were further verified by XRD (Fig. 3). Quartz (SiO_2) was found to be the major crystalline phase in all samples. Upon adding CaO, the P forms present in hydrochar were mainly $Ca_3(PO_4)_2$ and $Ca_5(PO_4)_3OH$, with $Ca_5(PO_4)_3OH$ being dominant. The addition of CaO to the hydrothermal reaction mixture initially produced a small amount of $Ca(OH)_2$, which led to an alkaline environment. In such conditions, $FePO_4$, $AlPO_4$, and $Mg_3(PO_4)_2$ were partially hydrolyzed to form $Fe(OH)_3$, $Al(OH)_3$ and $Mg(OH)_2$, releasing PO_4^{3-} (Zheng et al. 2020b). Furthermore, in alkaline environments, the released PO_4^{3-} does not form HPO_4^{2-} or $H_2PO_4^-$ (Li et al. 2022), binding with Ca^{2+} instead to form compounds such as $Ca_3(PO_4)_2$ and $Ca_5(PO_4)_3OH$ (Liu et al. 2021a). These stable Ca-P compounds contributed to the slow release of elemental P and higher P levels in the hydrochar (Zhu et al. 2023). As shown in Fig. 3b, the addition of $CaCl_2$ promoted P enrichment and the conversion of NAIP to AP in hydrochar, with $Ca_5(PO_4)_3Cl$ and Ca_2PO_4Cl being the main Ca-P compounds in the prepared hydrochar. Furthermore, $CaCl_2$ has been shown to exhibit unique molten salt properties, altering the original crystal structure and leading to the formation of $Ca_5(PO_4)_3Cl$ and Ca_2PO_4Cl (Fang et al. 2023), which increased the available P, making the biochar a potential phosphate fertilizer (Nan et al. 2023). The XRD patterns of SS-based hydrochar with MgO and $MgCl_2$ are illustrated in Fig. 3c, d. With the addition of increasing amounts of Mg-based salts, $Mg_3(PO_4)_2$ became the predominant P phase in the hydrochar, significantly enhancing the bioavailability

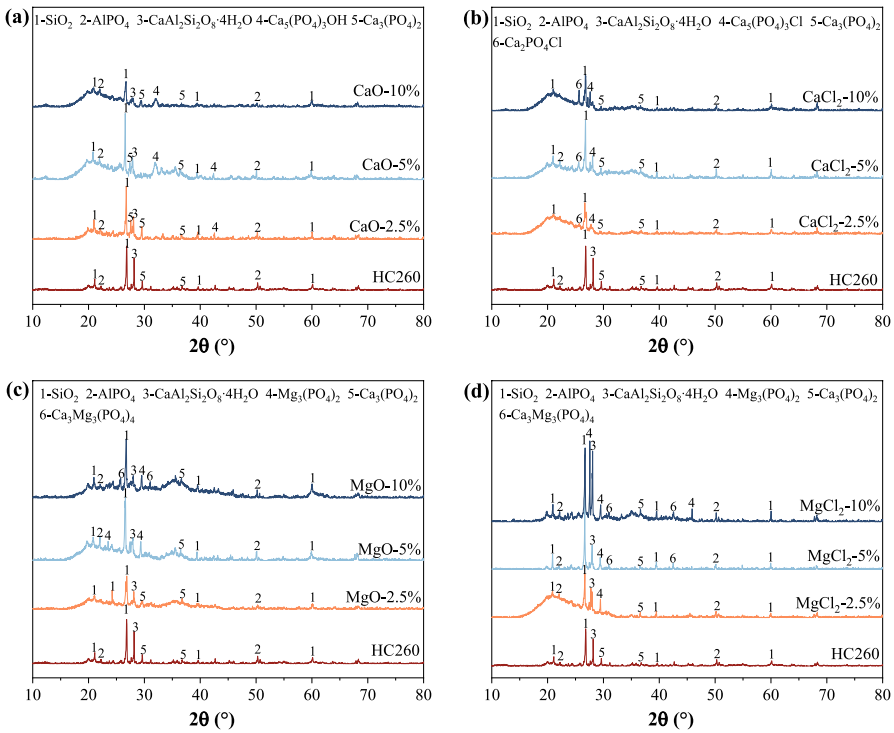


Fig. 3 XRD patterns of sludge-modified hydrochar with CaO (**a**), $CaCl_2$ (**b**), MgO (**c**), and $MgCl_2$ (**d**)

of P (Xia et al. 2020). Furthermore, with increasing Mg salt concentration, $Ca_3Mg_3(PO_4)_4$ appeared, a highly bioavailable P form, especially in acidic soils (Vogel et al. 2018). Thus, the addition of Ca/Mg salts promoted the formation of stable P-containing mineral structures in hydrochar, likely through a process where Ca and Mg compete with Fe and Al for P (Shi et al. 2021).

The XPS survey spectra of SS and hydrochars are presented in Fig. S6 (Supplementary Materials) and the XPS P 2p spectra are shown in Fig. 4, which can help to infer the possible compound forms of P in each sample. As illustrated in Fig. 4, the P 2p spectra of SS and the prepared hydrochars exhibited several peaks in the region of 133.1 eV, 134.0 eV and 135.1 eV, corresponding to PO_4, C-O-P, and metaphosphate (Meta-P), respectively. The percentages of the peak area (PPA), presented in Table S5 (Supplementary Materials), enabled the semi-quantitative assessment of P species. The PPAs of PO_4 in CaO-5%, $CaCl_2$−5%, MgO-5%, and $MgCl_2$−5% reached Maximum levels of 73.9%, 70.5%, 68.4% and 68.2, respectively, suggesting that the P-related peaks had red-shifted, indicating the formation of chemical bonds between P and the hydrochar matrix. The higher PPA of PO_4 in these samples reflects a greater amount of orthophosphate, which is the main form of P absorbed by plants from the soil (Zhu et al. 2018). Additionally, these results demonstrate that the co-hydrothermal carbonization of SS with Ca/Mg salts facilitated the transformation of organic phosphates into orthophosphate through the decomposition of associated organic groups.

FTIR spectroscopy was also used to confirm the change of P species in the sample (Fig. 5). The Ester-P bonds, including both Monoester-P and Diester-P, were identified by a characteristic peak at 1540 cm^{-1}, which was attributed to OP and was only detected in the raw sludge. The infrared band corresponding to Pyro-P ($P_2O_7^{4+}$) appeared at approximately 530 cm^{-1} in all samples (Kohale and Dhoble 2018). The P = O peak (Ortho-P) appeared at the wavenumbers of 1050 cm^{-1} bands, corresponding to symmetric P = O extensions (Elzinga and Sparks 2007). Following hydrothermal carbonization, the intensity of Ortho-P gradually increased, and this change was further enhanced by the addition of Ca/Mg salts. The findings from the FTIR spectra were consistent with the XPS analysis.

3.2 Ecotoxicological risk assessment based on heavy metal speciation

As shown in Fig. 6, the majority of heavy metals in all treatments were predominantly found in the oxidizable and residual fractions (F3 and F4). Moreover, different Ca/Mg salt treatments exhibited varying capacities to immobilize specific heavy metals. Notably, oxide-based salts (CaO and MgO) were more effective in reducing

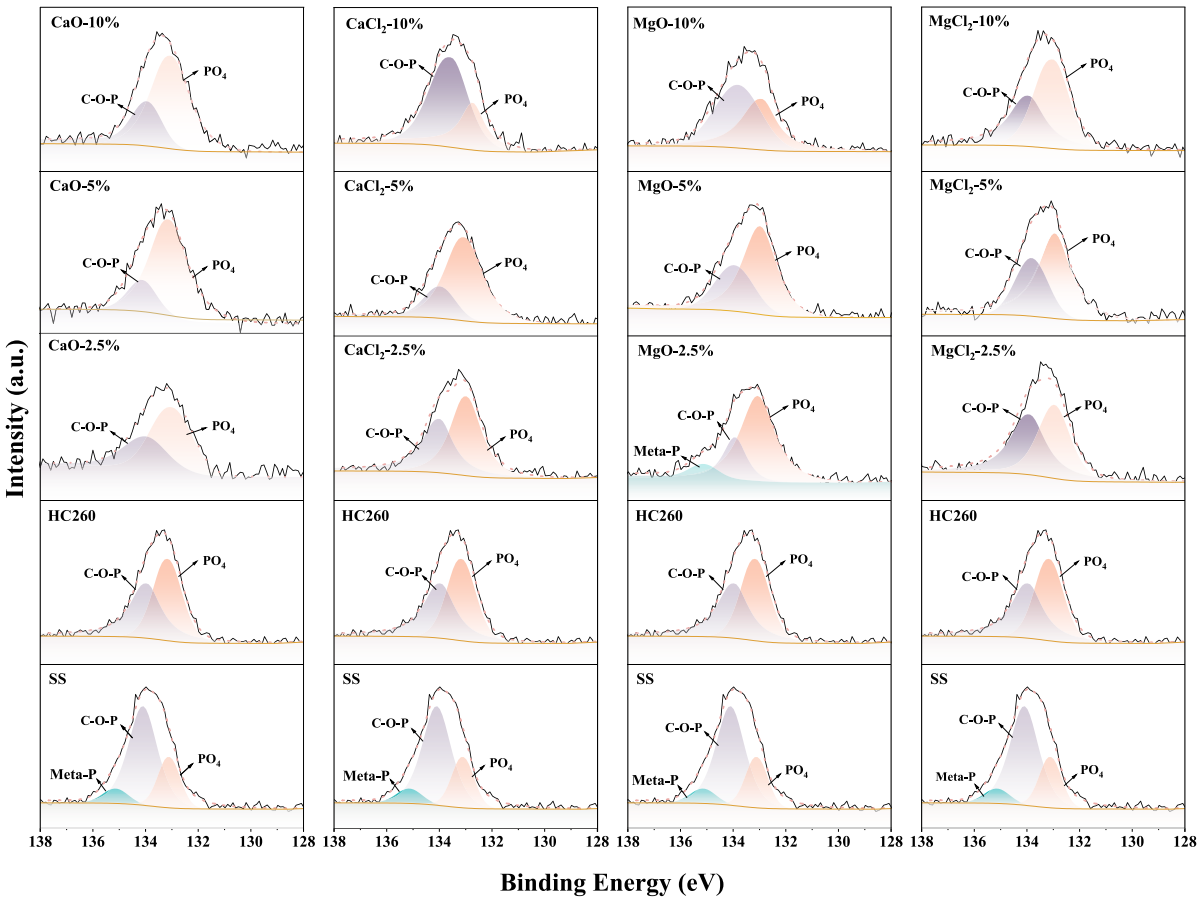


Fig. 4 XPS spectra of the P 2p orbital of raw SS and hydrochar prepared using different salt dosages

the proportions of the most mobile and toxic fractions (F1 + F2). For example, Cd and Zn-typically considered highly mobile metals showed markedly lower F1 + F2 proportions in the CaO and MgO groups compared to $CaCl_2$ and $MgCl_2$. This can be attributed to the alkaline nature of CaO and MgO, which increases the pH during pyrolysis and promotes the transformation of heavy metals into F4 fraction (Yang et al. 2020; Liu et al. 2021b). In contrast, treatments using chloride salts ($CaCl_2$ and $MgCl_2$) retained relatively higher proportions of exchangeable and reducible fractions for several metals. Nevertheless, the F3 and F4 fractions remained the predominant species in all treatments. Chloride exhibited a unique mechanism by promoting the volatilization of certain heavy metals through the formation of volatile chlorides during pyrolysis, thereby reducing their bioavailable forms. Additionally, Cl^- can react with metals in F1 fractions, converting them into more stable compounds within F4 fractions (Xia et al. 2020; Tian and Liu 2020; Galey et al. 2022). Therefore, these findings demonstrate that the type of Ca/Mg salt significantly influences the chemical speciation of heavy metals, reducing the ecological risks of hydrochar application.

3.3 Effect of hydrochars amendment on soil P and plant growth

3.3.1 Effect of hydrochars on Vigna radiata growth

To further confirm that Ca/Mg-based hydrochars is potentially suitable for application as a P fertilizer, this study assessed the effect of different hydrochar soil amendments on plant growth through a bioassay of *V. radiata* growth. As shown in Fig. 7a, compared to HC-260, the groups treated with Ca/Mg salts exhibited an increase in dry weight by 8.2%–46.9%, with the pronounced increase in fresh mass (Fig. 7b) suggesting that Ca/Mg-modified hydrochars not only promoted plant growth, but also significantly improved the water retention capacity of plants (Chen et al. 2022b). The impact of hydrochar amendments on the height of *V. radiata* plants was illustrated in Fig. 7c, showing that the Ca/Mg-based hydrochar significantly ($p < 0.05$) increased the height of *V. radiata* plants by 15.2% to 31.7% as compared to

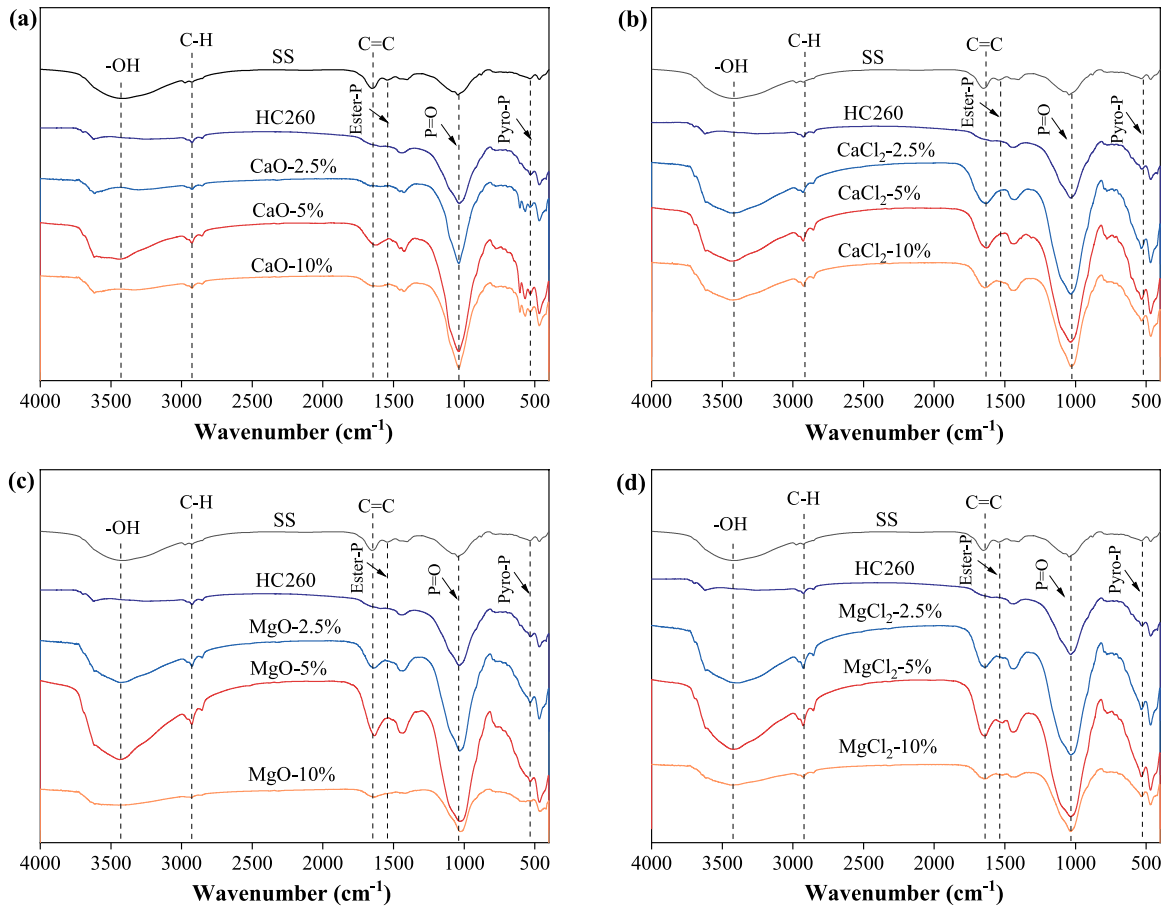


Fig. 5 FTIR spectra of sludge-modified hydrochar with CaO (**a**), $CaCl_2$ (**b**), MgO (**c**), and $MgCl_2$ (**d**) of raw SS and hydrochar prepared using different salt dosages

the control group. The higher biomass observed in the hydrochar-amended soil (Fig. 7b) can be attributed to the increased P availability, which provides essential nutrients from the P-rich biochar (Qiu et al. 2023). In addition, the increase in soil pH following biochar addition also promoted the release of surface-bound P (Chen et al. 2023).

In terms of the physiological characteristics of *V. radiata* plants, hydrochar amendments reduced the C_i of plants (Fig. 7d). The C_i decreased by 1.6% to 14.1% across all treatment groups, suggesting that as the photosynthetic demand increased due to the higher biomass, the concentration of CO_2 within the leaf declined due to greater levels of uptake (Wong et al. 1979; Medrano et al. 2015). Furthermore, G_s was significantly ($p < 0.05$) enhanced by hydrochar amendments, with an increase from 97.7% to 168.8% observed as compared to the control group (Fig. 7e). The improvement in G_s was attributed to the capacity for hydrochar to enhance soil moisture retention, thereby alleviating water stress and promoting the opening of stomata. This was consistent with the findings of a previously reported study, where improved soil water availability was linked to increased stomatal aperture, facilitating both CO_2 uptake and transpiration (Chaves et al. 2003). As illustrated in Fig. 7f, the chlorophyll content in plants from the treatment groups was higher than in the control group, with the HC-MgO and HC-$MgCl_2$ groups showing the most pronounced increases, rising by 32.6% and 31.1%, respectively. This enhancement was attributed to the addition of Mg salts, which significantly elevated the Mg concentration in soil, thereby promoting chlorophyll biosynthesis (Roy et al. 2022). Furthermore, the chlorophyll a/b ratio significantly ($p < 0.05$) increased in the treated groups, which is a key indicator of the light-harvesting efficiency of a plant. Specifically, the chlorophyll a/b ratios in the Ca/Mg-treated groups were 52.4%–61.3% higher than in the control group. This increase was likely due to the increased availability of key nutrients with the addition of Ca/Mg-composite hydrochars, promoting the synthesis of light-harvesting chlorophyll-protein complexes, as reported by Terashima and Hikosaka (1995).

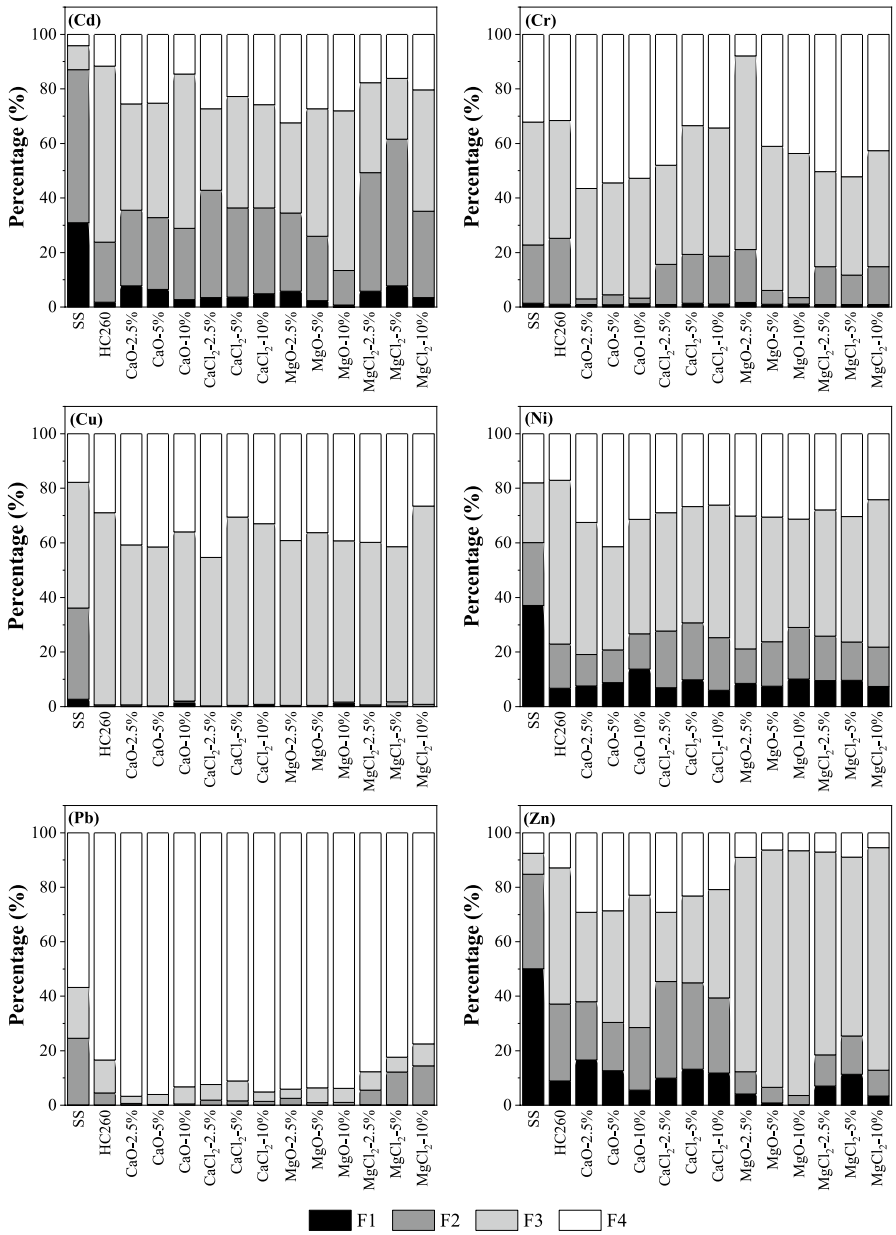


Fig. 6 The speciation and percentage of heavy metals in raw and hydrochars: F1 (the acid soluble/exchangeable fraction); F2 (the reducible fraction); F3 (the oxidizable fraction); and F4 (the residual fraction)

The growth of *V. radiata* with the addition of different P sources highlighted the distinct roles of Ca-P and Mg-P as P fertilizers. *V. radiata* plants treated with Mg-P exhibited a higher dry weight, fresh weight, and plant height. In addition, MgO achieved the most favorable treatment effect in terms of the physiological characteristics of *V. radiata* plants, indicating that the higher solubility of Mg-P allows for rapid P release from hydrochar and direct uptake by plants. This rapid effect would be particularly beneficial in scenarios where rapid growth is required, especially in acidic soils where the solubility of Mg-P would be further enhanced. In contrast, plants treated with Ca-P exhibited more moderate growth responses, which is consistent with the lower solubility and slower release of P from Ca-P, resulting in hydrochar conditioned by Ca salts being more suitable for use as a long-term, slow-release fertilizer. which can supporting crop growth beyond a single planting season. The stable growth and sustained nutrient availability provided by Ca-P, could help reduce the risk of P leaching and ensure prolonged plant development when used to modify hydrochar soil amendments.

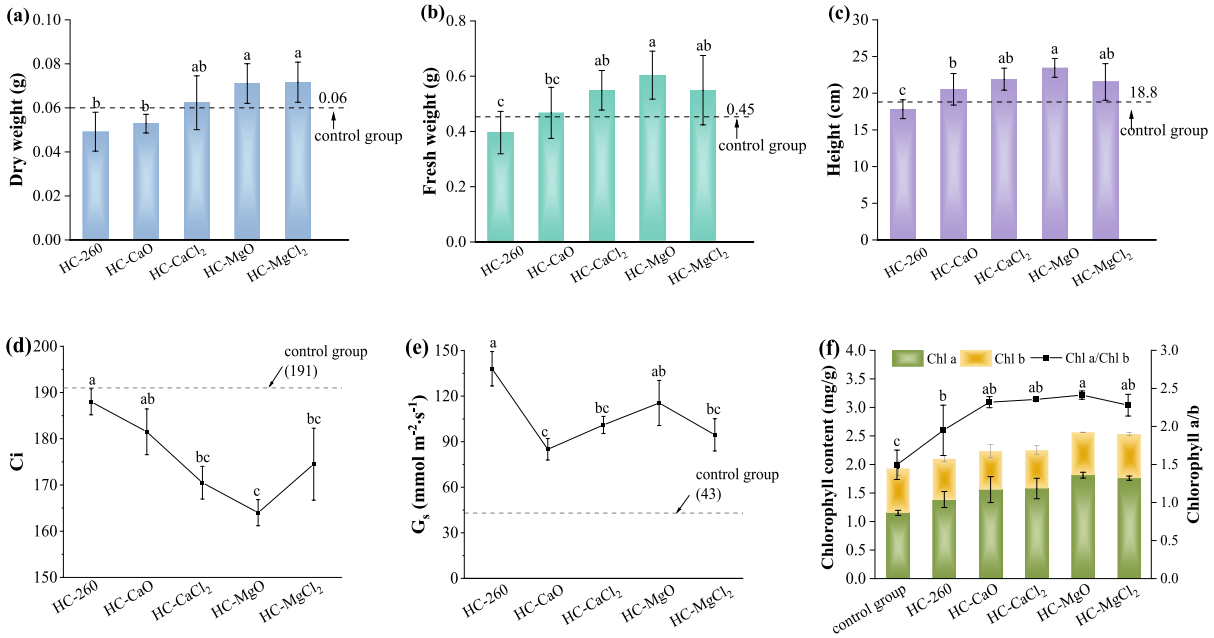


Fig. 7 Effects of Ca/Mg salts on *Vigna radiata* growth and photosynthetic parameters. **a** dried weight; **b** fresh weight; **c** height; **d** intercellular CO_2 concentration (C_i); **e** stomatal conductance (G_s); **f** chlorophyll content and chlorophyll a/b ratio. Letters indicate significant differences among the treatments using Tukey post hoc test

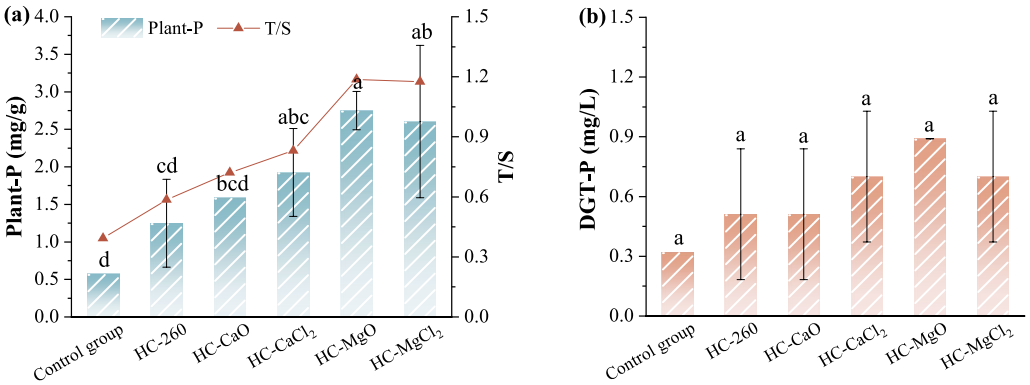


Fig. 8 **a** Plant P concentrations and P enrichment coefficients; **b** DGT P concentrations. Letters indicate significant differences among the treatments using Tukey post hoc test

3.3.2 P utilization by plants

The Plant-P content and the ratio of Soil-P to Plant-P are shown in Fig. 8a. The highest Plant-P content was detected in the HC-$CaCl_2$ group, followed by the HC-$MgCl_2$, HC-MgO and HC-CaO groups. Compared with the control group, the Plant-P content in soil amended with Ca/Ma salt modified hydrochars increased by 1.27- to 2.20-fold, suggesting that P availability was enhanced in the soil. The enrichment coefficient (T/S) of elements was established (Fig. 8a) to study the enrichment of P in *V. radiata* plants grown in different soil types, where T indicates the plant P content and S indicates the soil P content in the rhizospheric zone of the plant (Ding et al. 2021). In different treatment groups the T/S ratio value of P was ranked in the following order: HC-MgO > HC-$MgCl_2$ > HC-$CaCl_2$ > HC-CaO > HC-260 > control, indicating that plants grown in Mg-based hydrochar-amended soils have a strong capability to enrich P. The DGT-P content in soils is shown in Fig. 8b, showing that the DGT-P content in the control group was relatively low, in good agreement with the Plant-P concentrations detected across the soil samples (Fig. 8a). With the addition of different hydrochars, DGT-P

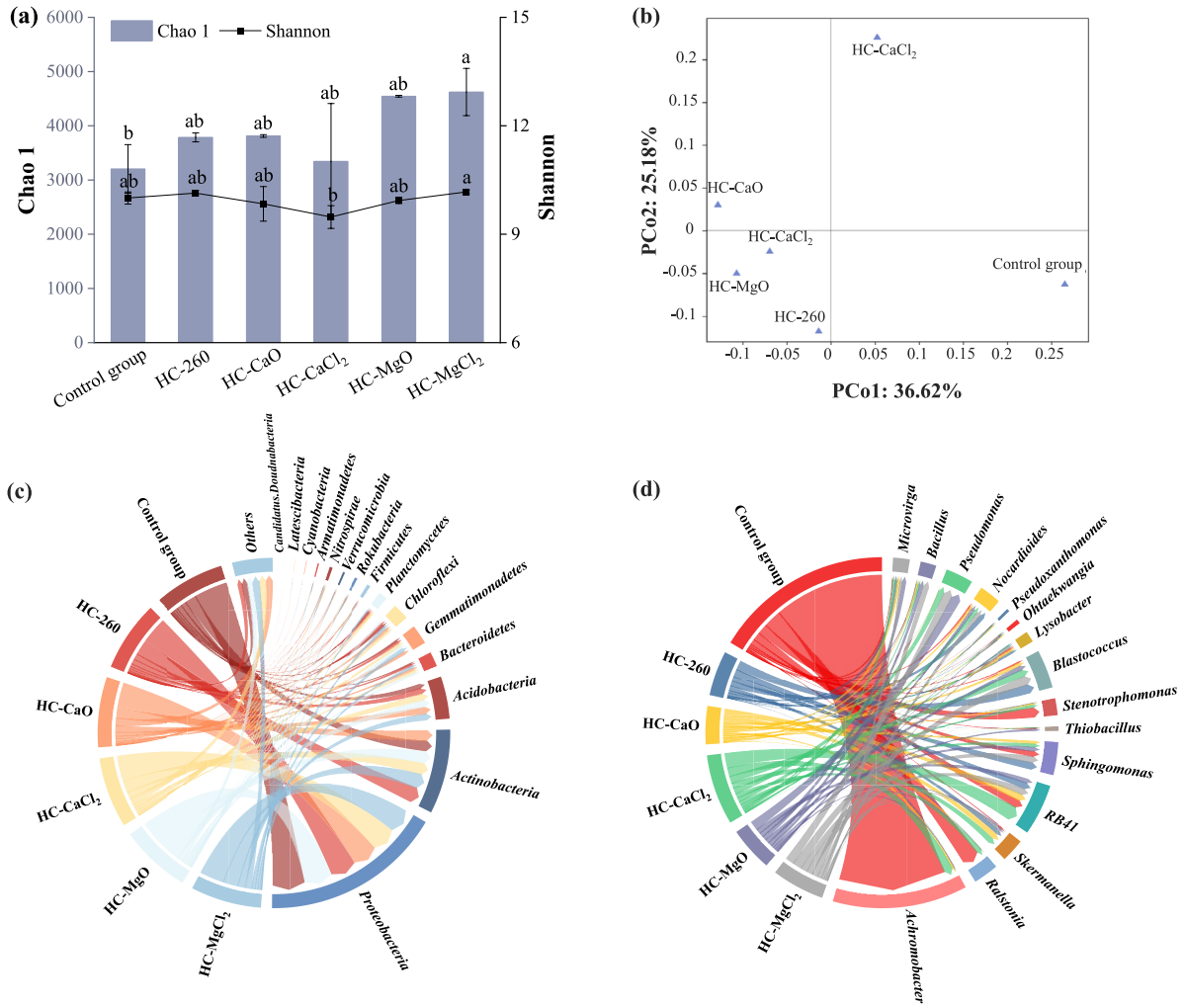


Fig. 9 **a** Alpha diversity analysis; **b** PCoA analysis based on the Bray–Curtis distance; **c** Relative abundance of bacteria at the phylum level (Top 15 in samples); **d** Relative abundance of bacteria at the genus level (Top 15 in samples). Letters indicate significant differences among the treatments using Tukey post hoc test

content increased up to 1.59- to 3.38 times that in the control group, with values ranging from 0.51 mg/L (HC-260) to 1.08 mg/L (HC-$CaCl_2$), which again suggests that Ca/Mg modification has the effect of increasing soil bioavailable P content. The correlation analysis between the total P content in *V. radiata* and soil P concentrations measured using different soil tests (Soil-P, Olsen-P and DGT-P) is shown in the Table S6.

3.4 Microbial and genetic responses to hydrochar in soil–plant systems

3.4.1 Effects of hydrochar on the microbial communities and bacterial diversity in soil

The Chao1 index significantly ($p < 0.05$) increased in rhizosphere soils with the addition of hydrochar materials (Fig. 9a), especially in the HC-$MgCl_2$ group. This suggests that $MgCl_2$-modified hydrochar had a particularly strong effect on the enhancement of microbial diversity. However, hydrochar has no significant influence on the Shannon index of the soil microbial community. By applying principal coordinate analysis (PCoA) to the Bray–Curtis dissimilarity measures, significant differences in bacterial community composition among different treatments were observed. Samples from the HC-CaO, HC-$CaCl_2$, HC-CaO, and HC-$MgCl_2$ treatment groups were significantly distinct from the control group PCo1 (36.62%), indicating significant alterations in the composition of the bacterial community with the application of hydrochar (Fig. 9b).

The variations in abundance of the top 15 dominant phyla among all samples were compared, as shown in Fig. 9c. *Proteobacteria* (39%–52%), *Actinobacteria* (17%–25%), *Acidobacteria* (8%–11%) and *Bacteroidetes* (2%–4%) were the predominant phyla in the soil, accounting

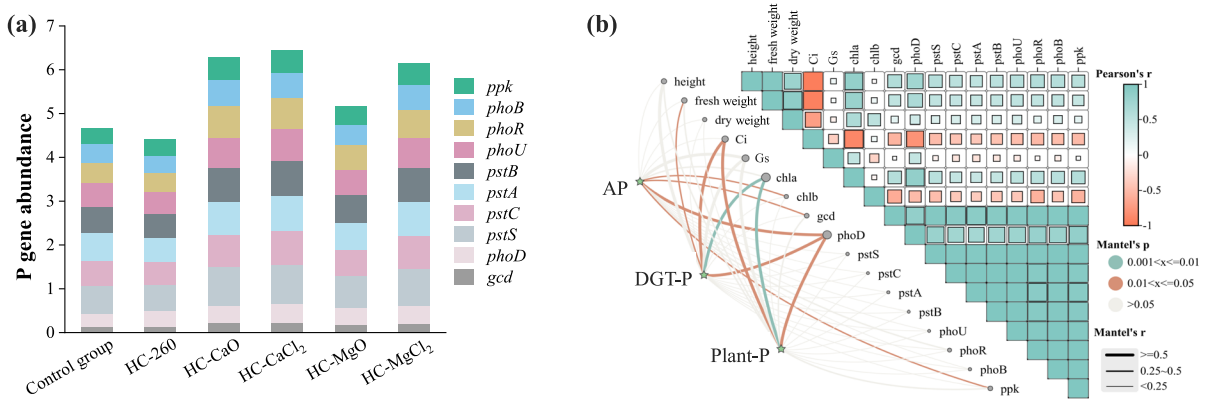


Fig. 10 **a** Abundance of P-cycling genes; **b** Correlations between P-cycling genes, plant growth index, and available P indicators. A pairwise comparison of rhizosphere soil properties is shown with a color denoting Pearson correlation coefficient. Edge width corresponds to the Mantel's r, and edge color indicates the statistical significance

for > 90% of the total bacterial community. The abundance of *Proteobacteria* in soils amended with hydrochars decreased by 15.4%–25.0% compared to the control group, while the abundance of *Actinobacteria*, *Acidobacteria*, and *Bacteroidetes* increased by 47.1%, 12.5%–37.5% and 50.0%–99.8%, respectively. *Actinobacteria* in soil can enhance soil P availability through phosphate solubility and enhanced phosphatase activity (Sun et al. 2020). *Acidophilus* and *Bacteroides* are bacterial phyla that are known to promote growth in plants, serving as P regulators by mineralizing organic P and converting insoluble P into soluble P (Ding et al. 2024). The increased abundance of *Actinobacteria*, *Acidophilus* and *Bacteroides* in the hydrochar-treated group helped to improve P availability in soil and promote plant growth.

The relative abundances of bacteria in soil samples at the genus level are shown in Fig. 9d. The addition of Ca/Mg-modified hydrochars significantly affected soil microbial communities, notably increasing the relative abundance of key P-solubilizing and mineralizing bacteria, thereby enhancing the soil microbial capacity for P activation and utilization. Specifically, Ca-modified hydrochars (HC-CaO and HC-$CaCl_2$) significantly ($p < 0.05$) enhanced the activity of bacteria such as *Skermanella* and *RB41*, which are widely associated with P mineralization and rapid nutrient cycling (Wang et al. 2022; Han et al. 2024). The relative abundance of *Skermanella* increased to 14.85% after HC-CaO treatment (as compared to 0.73% in the control group), showing a strong enrichment effect for this bacterial group. Meanwhile, the abundance of *RB41* was significantly increased to 23.55% by HC-$CaCl_2$ treatment ($p < 0.05$) from 9.69% in the control group. However, Ca salts modification is known to have a weak promotive effect on IP-solubilizing bacterial groups such as *Bacillus* (Torres et al. 2024), which accounted for only 2.63% in the HC-CaO group, similar to the 2.33% observed in the HC-260 group. In contrast, Mg salts modification (HC-MgO and HC-$MgCl_2$) achieved a higher level of enrichment of P-solubilizing bacteria such as *Pseudomonas* (Zhang et al. 2017) and *Bacillus* (Torres et al. 2024). For example, the abundance of *Pseudomonas* significantly ($p < 0.05$) increased to 23.92% after HC-MgO treatment, as compared to 0.09% in the control group, while the abundance of *Bacillus* also significantly ($p < 0.05$) increased to 12.63% after HC-$MgCl_2$ treatment, as compared to 0.24% in the control group. The above results suggest that Mg salts modification had the strongest overall effect in terms of promoting P solubilization and utilization.

3.4.2 Correlation between P-related genes and plant traits under different hydrochar treatments

The gene abundances related to microbial P metabolism are shown in Fig. 10a. Specifically, the abundances of OP mineralization (e.g., *phoD*), IP solubilization (e.g., *gcd* and *ppk*), IP transportation (e.g., *pst*), and P regulation (e.g., *phoU*, *phoR*, and *phoB*) genes were significantly increased in treatment group (Bergkemper et al. 2016; Guo et al. 2024; Liu et al. 2025a). Figure 10b presents the integrated results of Pearson correlation and Mantel test analyses among P-cycling genes, plant growth parameters, and P availability indicators. Among the functional genes, *phoD*, which is associated with the mineralization of organic phosphate esters, exhibited significant correlations with AP, DGT-P, and Plant-P (Mantel test, $0.01 < p < 0.05$). Specifically, AP showed significant correlations with chlb, *gcd*, *phoD*, and *ppk*, while DGT-P was strongly associated with fresh weight, *Ci*, chla, and *phoD*. Furthermore, Plant-P was significantly correlated with *Ci*, chla, and *phoD*. Notably, although *phoD* exhibited

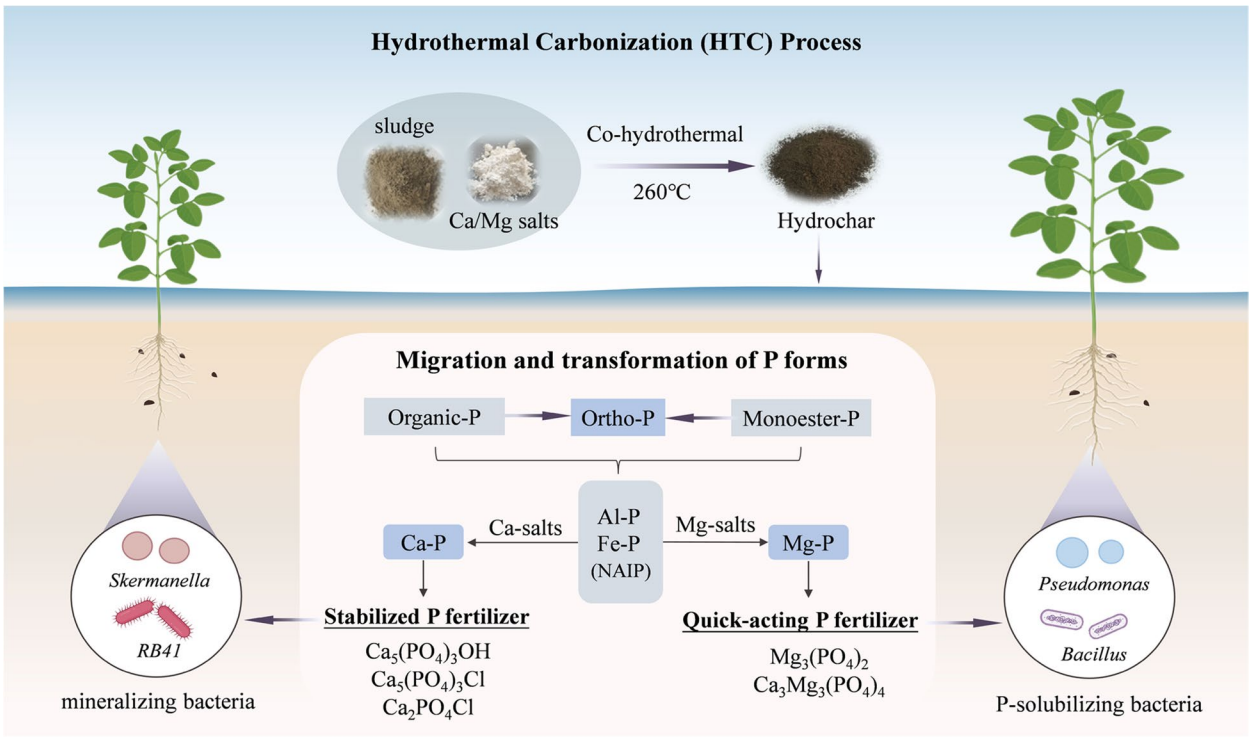


Fig. 11 Schematic diagram of the effect of Ca/Mg salt conditioned sludge-based hydrochar on the soil–plant-microbial system

a relatively low abundance, it played a critical role in enhancing soil P availability. These findings indicate that Ca/Mg-modified hydrochar may promote soil P cycling and plant growth by stimulating the expression of key genes involved in P solubilization and transport.

3.5 The principle and applied strategy of Ca/Mg salts modification of hydrochars as a phosphate fertilizer

The addition of Ca/Mg salts during sludge HTC significantly influences the transformation and migration patterns of various P species, directly affecting both P bioavailability and soil microbial diversity. As shown in Fig. 11, OP was converted into IP via organic matter decomposition in the HTC process. Accompanied by the hydrolysis of pyro-phosphate and dehydration of monoester phosphate, the IP content was further increased (Qian and Jiang 2014; Wang et al. 2024). Adding different Ca/Mg salts improved NAIP conversion to AP to varying degrees. In addition, Ca/Mg modification can also improve the P fixation capacity by increasing the carbon surface alkalinity, providing coordination sites and enhancing ion exchange capacity (Fang et al. 2020; Samaraweera et al. 2023). Notably, DGT-P and Plant-P measurements demonstrated that hydrochar addition enhanced the bioavailability of Pin soils, with this enhancement particularly crucial in soils that suffer from P fixation or low nutrient availability. Ca salt-modified hydrochars mainly enhanced the activity of mineralizing bacteria such as *Skermanella* and *RB41*, contributing to the improvement of P mineralization and circulation. In contrast, Mg salt modification tends to promote the enrichment of P-solubilizing bacterial communities such as *Pseudomonas* and *Bacillus*, making this approach suitable for improving the solubility and conversion capacity of P.

From the perspective of soil application, Ca salts formed stable alkaline crystalline phases (e.g., $Ca_5(PO_4)_3OH$, $Ca_5(PO_4)_3Cl$, and Ca_2PO_4Cl), which act as long-term slow release P fertilizer. This long-term property may support P supply over multiple crop seasons (Kätterer et al. 2019; Figueiredo et al. 2020). In contrast, Mg salts facilitate the formation of $Mg_3(PO_4)_2$ and $Ca_3Mg_3(PO_4)_4$, which readily dissolve under acidic conditions, favoring rapid P release and short-term effectiveness (Vogel et al. 2018). In addition, biochar generally contains some alkaline substances and thus can be used as an amendment to ameliorate soil acidity and raise soil pH, increasing the soil pH buffering capacity (Shi et al. 2017; Lu et al. 2022). This pH-responsive behavior and P release rate support the strategic use of Ca/Mg hydrochars to improve P efficiency across different soil types.

From an environmental point of view, Ca/Mg-modified hydrochar can significantly reduce the risk of P

leaching in soil and enhance microbial activity related to P, which helps to reduce the use of chemical fertilizers and improve soil quality (Samaraweera et al. 2023). In this study, the input of Ca/Mg salts was strictly controlled at 1000 mg/kg soil, and most were mineral-bound, minimizing potential ecological toxicity. Additionally, the aging of biochar may further influence its environmental impact, as it can enhance nutrient retention and microbial colonization but may also lead to acidification and mobilization of toxic metals such as Al^{3+}, thereby posing new environmental risks (Bai et al. 2020; Wang et al. 2020). Therefore, the long-term fate and ecological effects of Ca/Mg-modified hydrochar in soils warrant further investigation.

4 Conclusion

This study provided direct evidence of available P generation and utilization using Ca/Mg salt-conditioned hydrochar materials prepared from SS, showing promise as a phosphate fertilizer from the perspective of soil–plant-microbial systems. These findings suggest that both Ca and Mg treatment and HTC had a synergistic effect on P recovery and plant growth, However, the choice of additives used should depend on soil requirements and the plant growth stage, with the addition of Ca salts providing a stable, long-term P source, while the addition of Mg salts facilitated the rapid release of P, promoting short-term plant growth. However, the current study was conducted under controlled laboratory conditions with short-term pot experiments, future work should combine long-term field trials with AI-assisted modeling and expanded material screening (e.g., nanocomposites, membrane separation material) to predict real-world performance across diverse agroecosystems.

Supplementary Information

The online version contains supplementary material available at https://doi.org/10.1007/s44246-025-00228-2.

Supplementary Material 1.

Authors' contributions

All authors contributed to the study conception and design. Material preparation, data collection, and analysis were performed by Qian Zhao, Wei Guo, Yuhan Zhu, and Dongyue Li. The first draft of the manuscript was written by Qian Zhao and all authors commented on previous versions of the manuscript. All authors read and approved the final manuscript.

Funding

This work was supported by the Key Research and Development Project of Shandong (Grant No. 2020CXGC011404) and the National Natural Science Foundation of China (No. 41977325).

Data availability

The datasets used or analyzed during the current study are available from the corresponding author on reasonable requests.

Declarations

Competing interests

All authors declare that there are no competing interests.

Author details

[1]National Engineering Laboratory for Advanced Municipal Wastewater Treatment and Reuse Technology, Beijing University of Technology, Beijing 100124, China. [2]Key Laboratory of Marine Environment and Ecology, Ministry of Education and College of Environmental Science and Engineering, Ocean University of China, Qingdao 266100, China. [3]Institute of Environmental Processes and Pollution Control, School of Environment and Ecology, Jiangnan University, Wuxi 214122, China. [4]State Key Laboratory of Environmental Criteria and Risk Assessment, Chinese Research Academy of Environmental Sciences, Beijing 100012, China. [5]College of Chemistry and Chemical Engineering, Weifang University, Weifang 261061, China.

Received: 12 March 2025 Revised: 20 June 2025 Accepted: 25 June 2025
Published online: 17 September 2025

References

Adam C, Peplinski B, Michaelis M, Kley G, Simon F-G (2009) Thermochemical treatment of sewage sludge ashes for phosphorus recovery. Waste Manag 29:1122–1128. https://doi.org/10.1016/j.wasman.2008.09.011

Bai N, Zhang H, Zhou S, Sun H, Zhao Y, Zheng X, Li S, Zhang J, Lv W (2020) Long-term effects of straw return and straw-derived biochar amendment on bacterial communities in soil aggregates. Sci Rep 10:7891. https://doi.org/10.1038/s41598-020-64857-w

Bergkemper F, Schöler A, Engel M, Lang F, Krüger J, Schloter M, Schulz S (2016) Phosphorus depletion in forest soils shapes bacterial communities towards phosphorus recycling systems. Environ Microbiol 18:1988–2000. https://doi.org/10.1111/1462-2920.13188

Chaves MM, Maroco JP, Pereira JS (2003) Understanding plant responses to drought — from genes to the whole plant. Funct Plant Biol 30:239–264. https://doi.org/10.1071/fp02076

Chen G, Wang J, Yu F, Wang X, Xiao H, Yan B, Cui X (2022a) A review on the production of P-enriched hydro/bio-char from solid waste: Transformation of P and applications of hydro/bio-char. Chemosphere 301:134646. https://doi.org/10.1016/j.chemosphere.2022.134646

Chen J, Aihemaiti A, Xia Y, Yan F, Zhang Z (2022b) The effect of soil amendment derived from P-enhanced sludge pyrochar on ryegrass growth and soil microbial diversity. Sci Total Environ 813:152526. https://doi.org/10.1016/j.scitotenv.2021.152526

Chen H, Gao Y, Dong H, Sarkar B, Song H, Li J, Bolan N, Quin B, Yang X, Li F, Wu F, Meng J, Wang H, Chen W (2023) Chitin and crawfish shell biochar composite decreased heavy metal bioavailability and shifted rhizosphere bacterial community in an arsenic/lead co-contaminated soil. Environ Int 176:107989. https://doi.org/10.1016/j.envint.2023.107989

Cheng KH, Sun Z, Zhong W, Wang Z, Visser M, Liu S, Yan Z, Zhao Y, Zhang R, Zang J, Jin S, Wu J (2024) Enhancing wheat crop physiology monitoring through spectroscopic analysis of stomatal conductance dynamics. Remote Sens Environ 312:114325. https://doi.org/10.1016/j.rse.2024.114325

de Figueiredo CC, Pinheiro TD, de Oliveira LEZ, de Araujo AS, Coser TR, Paz-Ferreiro J (2020) Direct and residual effect of biochar derived from biosolids on soil phosphorus pools: A four-year field assessment. Sci Total Environ 739:140013. https://doi.org/10.1016/j.scitotenv.2020.140013

Ding S, Yu X, Zhang J, Yin Z, Zou Y, Wang G, Sheng L, He C (2021) Bioconcentration and translocation of elements regulate plant responses to water-salt conditions in saline-alkaline wetlands. Environ Exp Bot 183:104360. https://doi.org/10.1016/j.envexpbot.2020.104360

Ding S, Li J, Wang Y, He S, Xie H, Fu H, Feng Y, Shaheen SM, Rinklebe J, Xue L (2024) Manure derived hydrochar reduced phosphorus loss risk via an alteration of phosphorus fractions and diversified microbial community in rice paddy soil. Sci Total Environ 918:170582. https://doi.org/10.1016/j.scitotenv.2024.170582

Du B, Yu Z, Tian Y, Ma X (2021) Effects of baking soda on co-hydrothermal carbonization of sewage sludge and Chlorella vulgaris: Improved the environmental friendliness of hydrochar incineration process. J Environ Chem Eng 9:106404. https://doi.org/10.1016/j.jece.2021.106404
Egle L, Rechberger H, Krampe J, Zessner M (2016) Phosphorus recovery from municipal wastewater: An integrated comparative technological, environmental and economic assessment of P recovery technologies. Sci Total Environ 571:522–542. https://doi.org/10.1016/j.scitotenv.2016.07.019
El Bamiki R, Raji O, Ouabid M, Elghali A, Khadiri Yazami O, Bodinier JL (2021) Phosphate rocks: A review of sedimentary and igneous occurrences in Morocco. Minerals 11:1137. https://doi.org/10.3390/min11101137
Elser JJ (2012) Phosphorus: A limiting nutrient for humanity? Curr Opin Biotechnol 23:833–838. https://doi.org/10.1016/j.copbio.2012.03.001
Elzinga EJ, Sparks DL (2007) Phosphate adsorption onto hematite: An in situ ATR-FTIR investigation of the effects of pH and loading level on the mode of phosphate surface complexation. J Colloid Interface Sci 308:53–70. https://doi.org/10.1016/j.jcis.2006.12.061
Fang L, Yan F, Chen J, Shen X, Zhang Z (2020) Novel recovered compound phosphate fertilizer produced from sewage sludge and its incinerated ash. ACS Sustain Chem Eng 8:6611–6621. https://doi.org/10.1021/acssuschemeng.9b06861
Fang Z, Liu F, Li Y, Li B, Yang T, Li R (2021) Influence of microwave-assisted pyrolysis parameters and additives on phosphorus speciation and transformation in phosphorus-enriched biochar derived from municipal sewage sludge. J Clean Prod 287:125550. https://doi.org/10.1016/j.jclepro.2020.125550
Fang Z, Zhuang X, Zhang X, Li Y, Li R, Ma L (2023) Influence of paraments on the transformation behaviors and directional adjustment strategies of phosphorus forms during different thermochemical treatments of sludge. Fuel 333:126544. https://doi.org/10.1016/j.fuel.2022.126544
Galey B, Gautier M, Kim B, Blanc D, Chatain V, Ducom G, Dumont N, Gourdon R (2022) Trace metal elements vaporization and phosphorus recovery during sewage sludge thermochemical treatment – A review. J Hazard Mater 424:127360. https://doi.org/10.1016/j.jhazmat.2021.127360
Ghimirey V, Chaurasia J, Acharya N, Marahatta S, Devkota K (2024) Soil properties and yield of mung bean [VIGNA RADIATA (L.) WILCZEK] as influenced by tillage and phosphorous fertilizer management on sandy loam soil in Chitwan, Nepal. J Saudi Soc Agric Sci. https://doi.org/10.1016/j.jssas.2024.10.001
Ghosh P, Rathinasabapathi B, Ma LQ (2015) Phosphorus solubilization and plant growth enhancement by arsenic-resistant bacteria. Chemosphere 134:1–6. https://doi.org/10.1016/j.chemosphere.2015.03.048
González Medeiros JJ, Pérez Cid B, Fernández Gómez E (2005) Analytical phosphorus fractionation in sewage sludge and sediment samples. Anal Bioanal Chem 381:873–878. https://doi.org/10.1007/s00216-004-2989-z
Guan D-X, Williams PN, Luo J, Zheng JL, Xu HC, Cai C, Ma LQ (2015) Novel precipitated zirconia-based DGT technique for high-resolution imaging of oxyanions in waters and sediments. Environ Sci Technol 49:3653–3661. https://doi.org/10.1021/es505424m
Guo T, Zhang S, Song C, Zhao R, Jia L, Wei Z (2024) Response of phosphorus fractions transformation and microbial community to carbon-to-phosphorus ratios during sludge composting. J Environ Manage 360:121145. https://doi.org/10.1016/j.jenvman.2024.121145
Han H, Hu S, Zhang Y, He L, Abdullahi SA, Ma S, Deng Z, Wang Y, Su S, Xiang J (2021) Roles of dehydration conditioners on the formation of apatite phosphorus during the pyrolysis of various sludge. J Environ Chem Eng 9:105248. https://doi.org/10.1016/j.jece.2021.105248
Han H, Song P, Jiang Y, Fan J, Khan A, Liu P, Mašek O, Li X (2024) Biochar immobilized hydrolase degrades PET microplastics and alleviates the disturbance of soil microbial function via modulating nitrogen and phosphorus cycles. J Hazard Mater 474:134838. https://doi.org/10.1016/j.jhazmat.2024.134838
Hiscox JD, Israelstam GF (1979) A method for the extraction of chlorophyll from leaf tissue without maceration. Can J Bot 57:1332–1334. https://doi.org/10.1139/b79-163
House WA (1999) The physico-chemical conditions for the precipitation of phosphate with calcium. Environ Technol 20:727–733. https://doi.org/10.1080/09593332008616867
Jeon S, Kim D-J (2018) Enhanced phosphorus bioavailability and heavy metal removal from sewage sludge ash through thermochemical treatment with chlorine donors. J Ind Eng Chem 58:216–221. https://doi.org/10.1016/j.jiec.2017.09.028
Jordan-Meille L, Rubæk GH, Ehlert PaI, Genot V, Hofman G, Goulding K, Recknagel J, Provolo G, Barraclough P (2012) An overview of fertilizer-P recommendations in Europe: Soil testing, calibration and fertilizer recommendations. Soil Use Manag 28:419–435. https://doi.org/10.1111/j.1475-2743.2012.00453.x
Kätterer T, Roobroeck D, Andrén O, Kimutai G, Karltun E, Kirchmann H, Nyberg G, Vanlauwe B, Röing de Nowina K (2019) Biochar addition persistently increased soil fertility and yields in maize-soybean rotations over 10 years in sub-humid regions of Kenya. Field Crops Res 235:18–26. https://doi.org/10.1016/j.fcr.2019.02.015
Kohale RL, Dhoble SJ (2018) Optical performance of $Ca_2P_2O_7$: Ce^{3+} pyrophosphate phosphor synthesized via modified solid state diffusion. J Mol Struct 1170:18–23. https://doi.org/10.1016/j.molstruc.2018.05.065
Li R, Teng W, Li Y, Yin J, Zhang Z (2019) Transformation of phosphorus and stabilization of heavy metals during sewage sludge incineration: the effect of suitable additives and temperatures. Environ Sci Pollut Res 26:29917–29929. https://doi.org/10.1007/s11356-019-06146-2
Li B, Dinkler K, Zhao N, Ran X, Sobhi M, Dong R, Müller J, Xiong W, Huang G, Guo J, Oechsner H (2022) Response of phosphorus speciation to organic loading rates and temperatures during anaerobic co-digestion of animal manures and wheat straw. Sci Total Environ 838:155921. https://doi.org/10.1016/j.scitotenv.2022.155921
Li G, Ye R, Wu S, Liu X, Huang M, Guo J, Gao Y, Chen W, Ma Y (2025) Fly ash-doped biochar fabricated by pyrolysis and hydrothermal strategies: characteristics and potentialities of carbon sequestration. Carbon Res 4:23. https://doi.org/10.1007/s44246-024-00185-2
Liu H, Hu G, Basar IA, Li J, Lyczko N, Nzihou A, Eskicioglu C (2021a) Phosphorus recovery from municipal sludge-derived ash and hydrochar through wet-chemical technology: A review towards sustainable waste management. Chem Eng J 417:129300. https://doi.org/10.1016/j.cej.2021.129300
Liu L, Huang L, Huang R, Lin H, Wang D (2021b) Immobilization of heavy metals in biochar derived from co-pyrolysis of sewage sludge and calcium sulfate. J Hazard Mater 403:123648. https://doi.org/10.1016/j.jhazmat.2020.123648
Liu D, Zhang S, Zhuang W, Li K, Wang F, Li T, Chen D, Fan Q, Zhang Z, Tudi M, Che R (2025a) Reforestation significantly enriches soil microbial carbon, nitrogen, and phosphorus cycling genes but simplifies their co-occurrence network. Appl Soil Ecol 207:105935. https://doi.org/10.1016/j.apsoil.2025.105935
Liu X, Peng L, Deng P, Xu Y, Wang P, Tan Q, Zhang C, Dai X (2025b) Co-hydrothermal carbonization of sewage sludge and rice straw to improve hydrochar quality: Effects of mixing ratio and hydrothermal temperature. Bioresour Technol 415:131665. https://doi.org/10.1016/j.biortech.2024.131665
Lu RK (2000) Soil analytical methods of agronomic chemistry. Chin. Agric. Sci. Technol. Press, Beijing, pp 166–170
Lu H, Li K, Nkoh JN, Shi Y, He X, Hong Z, Xu R (2022) Effects of the increases in soil pH and pH buffering capacity induced by crop residue biochars on available Cd contents in acidic paddy soils. Chemosphere 301:134674. https://doi.org/10.1016/j.chemosphere.2022.134674
Ma S, Wang H, Gao X, Bian C, Zhu W (2025) Mitigating ammonia inhibition in anaerobic digestion with lignin-based carbon materials synthesized by hydrothermal carbonization. Carbon Res 4:20. https://doi.org/10.1007/s44246-024-00184-3
Mason SD, McLaughlin MJ, Johnston C, McNeill A (2013) Soil test measures of available P (Colwell, resin and DGT) compared with plant P uptake using isotope dilution. Plant Soil 373:711–722. https://doi.org/10.1007/s11104-013-1833-7
Medrano H, Tomás M, Martorell S, Flexas J, Hernández E, Rosselló J, Pou A, Escalona JM, Bota J (2015) From leaf to whole-plant water use efficiency (WUE) in complex canopies: Limitations of leaf WUE as a selection target. Crop J 3:220–228. https://doi.org/10.1016/j.cj.2015.04.002
Meng X, Huang Q, Gao H, Tay K, Yan J (2018) Improved utilization of phosphorous from sewage sludge (as Fertilizer) after treatment by low-temperature combustion. Waste Manag 80:349–358. https://doi.org/10.1016/j.wasman.2018.09.034
Mnthambala F, Tilley E, Tyrrel S, Sakrabani R (2021) Phosphorus flow analysis for Malawi: Identifying potential sources of renewable phosphorus recovery.

Resour Conserv Recycl 173:105744. https://doi.org/10.1016/j.resconrec.2021.105744
Murphy J, Riley JP (1962) A modified single solution method for the determination of phosphate in natural waters. Anal Chim Acta 27:31–36. https://doi.org/10.1016/S0003-2670(00)88444-5
Nahar K, Hedayati Marzbali M, Gbolahan Hakeem I, Sharma A, Chiang K, Surapaneni A, Gupta R, Ball A, Shah K (2024) Hydrothermal processing of primary, waste-activated, and digested sewage sludge: Products characterisation, fate of heavy metals and nutrients, and process integration. J Ind Eng Chem. https://doi.org/10.1016/j.jiec.2024.10.047
Nan H, Yang F, Li D, Cao X, Xu X, Qiu H, Zhao L (2023) Calcium enhances phosphorus reclamation during biochar formation: Mechanisms and potential application as a phosphorus fertilizer in a paddy soil. Waste Manag 162:83–91. https://doi.org/10.1016/j.wasman.2023.03.018
Pan B, Zhang Q, Du W, Zhang W, Pan B, Zhang Q, Xu Z, Zhang Q (2007) Selective heavy metals removal from waters by amorphous zirconium phosphate: Behavior and mechanism. Water Res 41:3103–3111. https://doi.org/10.1016/j.watres.2007.03.004
Qian T-T, Jiang H (2014) Migration of phosphorus in sewage sludge during different thermal treatment processes. ACS Sustain Chem Eng 2:1411–1419. https://doi.org/10.1021/sc400476j
Qiu J, Fernandes de Souza M, Robles-Aguilar AA, Apan A, Menzies NW, Chapman S, Mellor V, Dang YP (2023) Improving biochar properties by co-pyrolysis of pig manure with bio-invasive weed for use as the soil amendment. Chemosphere 312:137229. https://doi.org/10.1016/j.chemosphere.2022.137229
Roy Choudhury M, Christopher J, Das S, Apan A, Menzies NW, Chapman S, Mellor V, Dang YP (2022) Detection of calcium, magnesium, and chlorophyll variations of wheat genotypes on sodic soils using hyperspectral red edge parameters. Environ Technol Innov 27:102469. https://doi.org/10.1016/j.eti.2022.102469
Samaraweera H, Palansooriya KN, Dissanayake PD, Khan AH, Sillanpää M, Mlsna T (2023) Sustainable phosphate removal using Mg/Ca-modified biochar hybrids: Current trends and future outlooks. Case Stud Chem Environ Eng 8:100528. https://doi.org/10.1016/j.cscee.2023.100528
Santner J, Zhang H, Leitner D, Schnepf A, Prohaska T, Puschenreiter M, Wenzel WW (2012) High-resolution chemical imaging of labile phosphorus in the rhizosphere of *Brassica napus* L. cultivars. Environ Exp Bot 77:219–226. https://doi.org/10.1016/j.envexpbot.2011.11.026
Shi R, Hong Z, Li J, Jiang J, Baquy M, Xu R, Qian W (2017) Mechanisms for increasing the pH buffering capacity of an acidic ultisol by crop residue-derived biochars. J Agric Food Chem 65:8111–8119. https://doi.org/10.1021/acs.jafc.7b02266
Shi Y, Luo G, Rao Y, Chen H, Zhang S (2019) Hydrothermal conversion of dewatered sewage sludge: Focusing on the transformation mechanism and recovery of phosphorus. Chemosphere 228:619–628. https://doi.org/10.1016/j.chemosphere.2019.04.109
Shi Y, Chen Z, Cao Y, Fan J, Clark JH, Luo G, Zhang S (2021) Migration and transformation mechanism of phosphorus in waste activated sludge during anaerobic fermentation and hydrothermal conversion. J Hazard Mater 403:123649. https://doi.org/10.1016/j.jhazmat.2020.123649
Six L, Pypers P, Degryse F, Smolders E, Merckx R (2012) The performance of DGT versus conventional soil phosphorus tests in tropical soils - An isotope dilution study. Plant Soil 359:267–279. https://doi.org/10.1007/s11104-012-1192-9
Sun K, Han L, Yang Y, Xia X, Yang Z, Wu F, Li F, Feng Y, Xing B (2020) Application of hydrochar altered soil microbial community composition and the molecular structure of native soil organic carbon in a paddy soil. Environ Sci Technol 54:2715–2725. https://doi.org/10.1021/acs.est.9b05864
Terashima I, Hikosaka K (1995) Comparative ecophysiology of leaf and canopy photosynthesis. Plant Cell Environ 18:1111–1128. https://doi.org/10.1111/j.1365-3040.1995.tb00623.x
Tian T, Liu Q-S (2020) Effects of added salts on sewage sludge char characteristics and heavy metal behaviors. J Anal Appl Pyrolysis 146:104774. https://doi.org/10.1016/j.jaap.2020.104774
Torres P, Altier N, Beyhaut E, Fresia P, Garaycochea S, Abreo E (2024) Phenotypic, genomic and *in planta* characterization of *Bacillus sensu lato* for their phosphorus biofertilization and plant growth promotion features in soybean. Microbiol Res 280:127566. https://doi.org/10.1016/j.micres.2023.127566
Vogel C, Rivard C, Wilken V, Muskolus A, Adam C (2018) Performance of secondary P-fertilizers in pot experiments analyzed by phosphorus X-ray absorption near-edge structure (XANES) spectroscopy. Ambio 47:62–72. https://doi.org/10.1007/s13280-017-0973-z
Vogel C, Sekine R, Steckenmesser D, Lombi E, Steffens D, Adam C (2017) Phosphorus availability of sewage sludge-based fertilizers determined by the diffusive gradients in thin films (DGT) technique. J Plant Nutr Soil Sci 180(5):594-601. https://doi.org/10.1002/jpln.v180.5.10.1002/jpln.201600531
Wang L, Chang Y, Liu Q (2019) Fate and distribution of nutrients and heavy metals during hydrothermal carbonization of sewage sludge with implication to land application. J Clean Prod 225:972–983. https://doi.org/10.1016/j.jclepro.2019.03.347
Wang L, O'Connor D, Rinklebe J, Ok YS, Tsang DC, Shen Z, Hou D (2020) Biochar aging: Mechanisms, physicochemical changes, assessment, and implications for field applications. Environ Sci Technol 54:14797–14814. https://doi.org/10.1021/acs.est.0c04033
Wang K, Qiu Z, Zhang M, Li X, Fang X, Zhao M, Shi F (2022) Effect of afforestation mode on rhizosphere soil physicochemical properties and bacterial community structure of two major tree species in Xiong'an New Area. For Ecol Manag 520:120361. https://doi.org/10.1016/j.foreco.2022.120361
Wang X, Mašek O, Li H, Yu F, Wurzer C, Wang J, Yan B, Cui X, Chen G, Hou LA (2024) Coupling electrokinetic technique with hydrothermal carbonization for phosphorus-enriched hydrochar production and heavy metal separation from sewage sludge. Chem Eng J 481:148144. https://doi.org/10.1016/j.cej.2023.148144
Wang L, Liu J, Jiang Y, Zhang T, Wang M, Yang D, Qiu F (2025) Trash to treasure: From waste sludge to phosphorus slow-release fertilizer. J Environ Chem Eng 13:116926. https://doi.org/10.1016/j.jece.2025.116926
White S, Cordell DJ, Moore DD (2010) Securing a sustainable phosphorus future for Australia: implications of global phosphorus scarcity and possible solutions. Inst Sust Futures pp 1–47. http://hdl.handle.net/10453/35033
Wong SC, Cowan IR, Farquhar GD (1979) Stomatal conductance correlates with photosynthetic capacity. Nature 282:424–426. https://doi.org/10.1038/282424a0
Wu B, Wan J, Zhang Y, Pan B, Lo IM (2020) Selective phosphate removal from water and wastewater using sorption: Process fundamentals and removal mechanisms. Environ Sci Technol 54:50–66. https://doi.org/10.1021/acs.est.9b05569
Wu Y, Li D, Li J, Xie C, Liang D, Ding F (2025) Research on optimizing DO and aerobic HRT for the treatment of low C/N urban wastewater using the SNEDPR-AGSBR system. J Inner Mongolia Univ Technol (Nat Sci Ed) 44:193–201
Xia Y, Tang Y, Shih K, Li B (2020) Enhanced phosphorus availability and heavy metal removal by chlorination during sewage sludge pyrolysis. J Hazard Mater 382:121110. https://doi.org/10.1016/j.jhazmat.2019.121110
Xu Y, Yang F, Zhang L, Wang X, Sun Y, Liu Q, Qian G (2018) Migration and transformation of phosphorus in municipal sludge by the hydrothermal treatment and its directional adjustment. Waste Manag 81:196–201. https://doi.org/10.1016/j.wasman.2018.10.011
Xu Y, Chen J, Yang F, Fang Y, Qian G (2021) Transformation of phosphorus by $MgCl_2$ and $CaCl_2$ during sewage sludge incineration. Environ Sci Pollut Res 28:60268–60275. https://doi.org/10.1007/s11356-021-13859-w
Yang Y-Q, Cui M-H, Ren Y-G, Guo JC, Zheng ZY, Liu H (2020) Towards understanding the mechanism of heavy metals immobilization in biochar derived from co-pyrolysis of sawdust and sewage sludge. Bull Environ Contam Toxicol 104:489–496. https://doi.org/10.1007/s00128-020-02801-4
Yogev U, Vogler M, Nir O, Londong J, Gross A (2020) Phosphorous recovery from a novel recirculating aquaculture system followed by its sustainable reuse as a fertilizer. Sci Total Environ 722:137949. https://doi.org/10.1016/j.scitotenv.2020.137949
Zehetner F, Wuenscher R, Peticzka R, Unterfrauner H (2018) Correlation of extractable soil phosphorus (P) with plant P uptake: 14 extraction methods applied to 50 agricultural soils from Central Europe. Plant Soil Env 64:. https://doi.org/10.17221/70/2018-PSE
Zhang G, Wang L, Li J, Zhou Y (2017) Pseudonocardia profundimaris sp. nov., isolated from marine sediment. Int J Syst Evol Microbiol 67:1693–1697. https://doi.org/10.1099/ijsem.0.001849

Zhang X, Zhang H, Huang S (2024) Synthesis of Sn_3O_4/g-C_3N_4 composites and the photocatalytic degradation of methyl orange. J Inner Mongolia Univ Technol (Nat Sci Ed) 43:373–378
Zhao Q, Guo W, Wang B, Zhang X, Li J (2024) Effect of different calcium salts on phosphorus availability and immobilization of heavy metals in municipal sludge derived biochar. J Water Process Eng 57:104708. https://doi.org/10.1016/j.jwpe.2023.104708
Zheng X, Jiang Z, Ying Z, Ye Y, Chen W, Wang B, Dou B (2020a) Migration and transformation of phosphorus during hydrothermal carbonization of sewage sludge: Focusing on the role of pH and calcium additive and the transformation mechanism. ACS Sustain Chem Eng 8:7806–7814. https://doi.org/10.1021/acssuschemeng.0c00031
Zheng X, Ye Y, Jiang Z, Ying Z, Ji S, Chen W, Wang B, Dou B (2020b) Enhanced transformation of phosphorus (P) in sewage sludge to hydroxyapatite via hydrothermal carbonization and calcium-based additive. Sci Total Environ 738:139786. https://doi.org/10.1016/j.scitotenv.2020.139786
Zhu J, Li M, Whelan M (2018) Phosphorus activators contribute to legacy phosphorus availability in agricultural soils: A review. Sci Total Environ 612:522–537. https://doi.org/10.1016/j.scitotenv.2017.08.095
Zhu Y, Zhao Q, Li D, Li J, Guo W (2022) Performance comparison of phosphorus recovery from different sludges in sewage treatment plants through pyrolysis. J Clean Prod 372:133728. https://doi.org/10.1016/j.jclepro.2022.133728
Zhu Y, Zhao Q, Li D, Li J, Guo W (2023) Enhanced recovery of phosphorus in sewage sludge-derived biochar with $CaCO_3$: Phosphorus speciation and slow-release phosphorus behavior. Sep Purif Technol 311:123325. https://doi.org/10.1016/j.seppur.2023.123325

Publisher's Note

Springer Nature remains neutral with regard to jurisdictional claims in published maps and institutional affiliations.